Simplified Vehicle Control Concept for a Lift Plus Cruise eVTOL Vehicle

John Kaneshige* Thomas Lombaerts† Kimberlee Shish‡ Michael Feary§
NASA Ames Research Center, Moffett Field, CA 94035

Electric Vertical Takeoff and Landing (eVTOL) vehicles have the potential to enable cost effective Urban Air Mobility (UAM) applications. These concepts may also pose several challenging handling and control problems, which must be addressed prior to safe and efficient urban operations. This paper investigates a simplified vehicle control concept that is designed to address some of these challenges for a conceptual Lift Plus Cruise vehicle. This concept also includes several variations of a transition-to-hover function, designed to assist pilots in capturing and maintaining a stabilized hover prior to landing. The different simplified control architectures for this concept are presented along with preliminary findings. Preliminary results show that the simplified control concept can be effective in assisting pilots to achieve safe and reliable hover landings, and that transition-to-hover functions have the potential of reducing workload while increasing accuracy. A follow on evaluation will be performed in the Vertical Motion Simulator (VMS) at NASA Ames Research Center. The planned tests will focus on more operationally representative scenarios, while building upon these operations with additional test cases exploring variations in glidepath angles and wind conditions.

Nomenclature

α	angle of attack [rad]
β	sideslip angle [rad]
$\mathbf{\Omega}$	rotation matrix
χ	track angle [rad]
Δ	difference / change
δ	deflection [rad]
γ	flight path angle [rad]
ϕ	bank angle [rad]
ψ	yaw angle [rad]
τ	time constant [s]
$\dot{h}$	climb/sink rate [ft/s]
$\dot{z}$	earth referenced vertical speed [ft/s]
$\overline{q}$	dynamic pressure, $= \frac{1}{2}\rho V_{\text{TAS}}^2$ [lbs/(ft s^2)]
C	coefficient [-]
D	drag [lbs ft/s^2]
dt	time step [s]
E	distance East [ft]
g	gravitational acceleration [ft/s^2]
h	altitude [ft]
K	controller gain [-]
L	lift [lbs ft/s^2]
m	mass [lbs]
N	distance North [ft]
n	load factor [-]
r	yaw rate [rad/s]
R_e	Earth radius [ft]
S	wing surface area [ft^2]
T	Thrust [lbs ft/s^2]
u	forward velocity component [ft/s]
V	speed [kts]
v	lateral velocity component [ft/s]
W	weight [lbs ft/s^2]
w	vertical speed component [ft/s]
X	distance along the nose X-axis [ft]
Y	distance along the wing Y-axis [ft]
Y	lateral axis or lateral force [lbs ft/s^2]
Z	vertical axis
lat	latitude [deg]
lon	longitude [deg]
B or b	body referenced
0	at sea level
crab	crab angle
aero	aerodynamic
env	envelope protected
lim	limited
pos	position
TAS	true airspeed
TC	turn coordination
thr	throttle

*Computer Engineer, Intelligent Systems Division, Mail Stop 269-1, AIAA member, email: john.t.kaneshige@nasa.gov.
†Aerospace Research Engineer, KBR, Intelligent Systems Division, Mail Stop 269-1, AIAA Associate Fellow, email: thomas.lombaerts@nasa.gov.
‡Aerospace Engineer, Intelligent Systems Division, Mail Stop 269-1, AIAA member, email: kimberlee.h.shish@nasa.gov.
§Aerospace Technologist, Human Systems Integration Division, Mail Stop 262-1, AIAA member, email: michael.s.feary@nasa.gov.

I. Introduction

Winged electric Vertical Takeoff and Landing (eVTOL) vehicles that can takeoff and land vertically like a helicopter and cruise like an airplane have the potential of increasing operational capabilities while maintaining a high degree of efficiency. Some designs have separate vertical and forward propulsion systems (e.g., a lift plus cruise vehicle), others have a tilting propulsion system (e.g., a tilt-rotor or tilt-wing vehicle), and hybrid designs have a combination of both concepts (e.g., with both vertical and tilting propulsion systems) [1]. During low speed and hover maneuvering, the vertical propulsion system provides the primary source of lift and maneuvering. As these vehicles transition between hover and forward flight, the vertical and/or tilting propulsion systems can be used to compensate for the changing amount of lift produced by the wings (e.g., to prevent the vehicles from stalling). Once sufficient airspeed is obtained, these vehicles can be controlled by manipulating traditional flight control surfaces. Upon reaching forward flight, the wings can produce all of the necessary lift, so the vertical propulsion systems can stop and/or the tilting propulsion systems can rotate fully forward.

Like all eVTOL vehicles, winged eVTOL vehicles suffer from slow response times during low speed and hover maneuvering. This is due to the multiple lifting rotor configuration that enables maneuvering by manipulating the thrust produced by individual rotors. Unlike a helicopter, the individual rotor blades are not cyclically controlled (i.e., so that it will have the same angle of incidence as it passes the same point in the cycle). Some rotors use a fixed blade pitch design, and manipulate thrust by modifying rotor speed (similar to smaller quadcopter drones). Other rotors use a variable blade pitch design, and manipulate thrust by collectively modifying the pitch angle of all the blades on an individual rotor (similar to the collective control of a helicopter). The latter has the advantage of faster rotor response times, but at a higher weight penalty [2]. However, both designs will typically have significantly slower maneuvering response times compared to a conventional helicopter.

Compared to multicopters, winged eVTOL vehicles are more susceptible to wind changes (e.g., due to gusts or changes in the vehicle's orientation with respect to the wind). As these vehicles transition between hover and forward flight, they will also encounter significant aerodynamic changes (e.g., the amount of lift produced by the wings and the amount of stabilizing pitch and yaw moments produced by the horizontal and vertical tails). As a result, these vehicles will respond differently as they transition between hover and forward flight. While these vehicles may be stable in forward flight, they are by design inherently unstable in hover and warrant the use of indirect flight control systems to provide stability and control augmentation. Furthermore, the slow response (at low speeds and hover) coupled with the changing nature of flight (when transitioning between hover and forward flight) may also necessitate higher-level outer loop control systems with a simpler pilot interface.

Simplified Vehicle Operations (SVO) is a term adopted by the aviation community for "the use of automation to reduce the number of skills a pilot or operator of an aircraft must acquire to achieve the required level of operational safety." [3] The term Simplified Vehicle Controls (SVC) is meant to convey a subset that focuses on the aircraft handling skill category. The SVC concept described in this paper was inspired by previously developed ideas. The 'Unified' control concept was initially developed specifically for VTOL vehicles by the UK's RAE (Royal Aircraft Establishment) in the 1970's and 80's [4]. It was first tested on the Vectored thrust Aircraft Advanced Control (VAAC) for the AV-8B Harrier [5], and this concept was recently further developed and implemented in the F-35B Lightning II [6, 7]. Another concept is based on the so-called 'E-Z Fly' control concept, developed at NASA Langley in the 1990's [8]. This concept decoupled the flight controls of a general aviation aircraft. This decoupling made the airplane "easy to fly", even for novice pilots. Both concepts have been developed further and adapted specifically for application in winged eVTOL vehicles in the context of UAM operations [9–11].

This paper examines an SVC concept with several different Assistive Hover Automation (AHA) concepts, along with corresponding pilot interfaces (i.e., inceptor implementations and display elements), to evaluate the effectiveness in compensating for control-related challenges of a conceptual Lift Plus Cruise (LPC) vehicle. The outline of this paper is as follows. First, the LPC vehicle model is described in Sec. II. Next, the SVC system is discussed in Sec. III. Thereafter, Sec. IV describes the simulation tests, with some specific test results. Finally, the paper wraps up with a summary and conclusions in Sec. V.

II. Lift Plus Cruise Vehicle

The Lift Plus Cruise (LPC) conceptual model was designed by NASA's Revolutionary Vertical Lift Technology (RVLT) project [12]. The vehicle is designed to takeoff and land vertically using lifting rotors, and to cruise in forward flight with the lifting rotors stowed. The vehicle can optimize power consumption efficiency by staying on the wing as long as possible. As a result, the proposed operational concept is to quickly accelerate just after takeoff, and to quickly decelerate to hover just prior to landing. An overview of the vehicle model is provided in Sec. II.A, and a description of the different flight regimes the vehicle experiences as it transitions between hover and forward flight is given in Sec. II.B.

A. Vehicle Model

The vehicle has a design gross weight of 6,000 lbs (with a payload of 1,000 lbs), range of 50 nautical miles at 100 knots (with a 20 minute reserve), and maximum speed of 120 knots. It has eight lifting rotors and one pusher propeller, as shown in Fig. 1. The vehicle also has flight control surfaces consisting of two ailerons, an elevator and a rudder. The lifting rotors and the pusher propeller are of a variable blade pitch angle design, and operate at a constant number of Rotations Per Minute (RPM). The amount of thrust produced by each rotor and the propeller can be independently manipulated by collectively adjusting the pitch angle of the blades. Collectively manipulating all rotors (1-8) will adjust the force along the heave axis. Manipulating the forward rotors (1-4) in the opposite direction as the rear rotors (5-8) will generate a pitch moment. Manipulating the left rotors (1-2, 5-6) in the opposite direction as the right rotors (3-4, 7-8) will generate a roll moment. Manipulating the counterclockwise spinning rotors (1, 3, 6, 8) in the opposite direction as the clockwise spinning rotors (2, 4, 5, 7) will generate a yaw moment. In forward flight, the lifting rotors are stopped at a neutral position and the vehicle is controlled using flight control surfaces, with the pusher propeller providing forward propulsion. The pusher propeller can also achieve up to 10 degrees of negative blade pitch angles so that limited reverse thrust is available for improving deceleration capability when needed. Without the lifting rotors, the stall speed of the vehicle is approximately 80 knots.

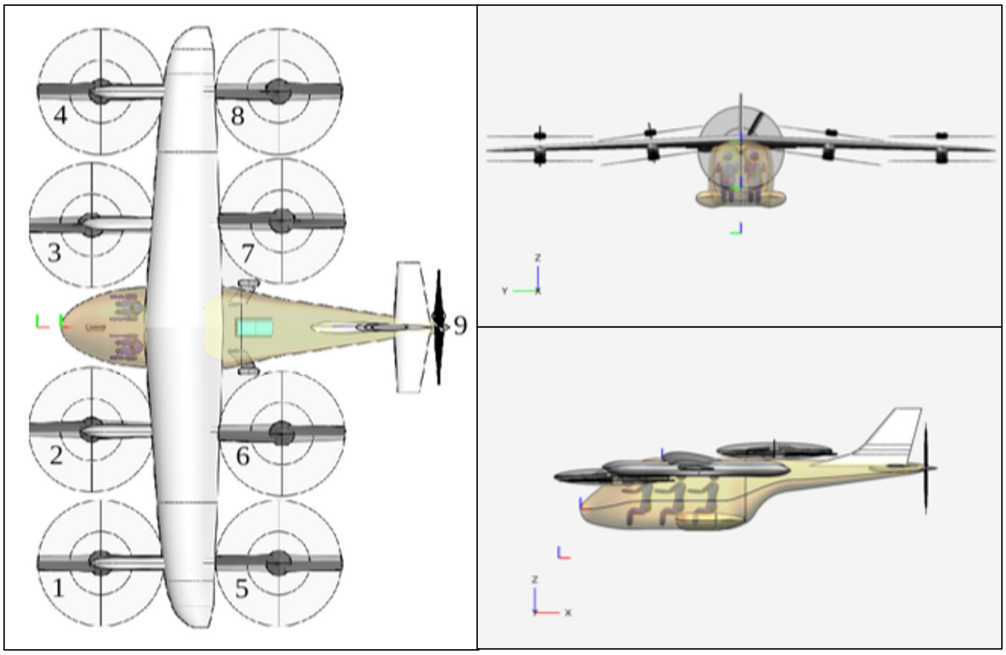

Fig. 1 Lift Plus Cruise (LPC) concept vehicle

The dynamic model was generated by Advanced Rotorcraft Technology (ART) using FlightLAB [13, 14]. This model was integrated into a flight simulation environment that was designed to enable rapid integration and evaluation of new vehicle models. The original quasi-Linear Parameter Varying (qLPV, a common rotorcraft representation [15, 16]) model was modified to apply nonlinear kinematic and gravitational terms (in place of linearized terms). The model inputs consist of the collective pitch angle for each lifting rotor and the pusher propeller, and deflection angles for the ailerons, elevator and rudder. The final simulation model also includes (1st and 2nd order) actuator models, a gear/ground model, a NASA Dryden-based turbulence model and a FAA-based wind gust model [17]).

B. Flight Regimes

The aircraft is described as being in the hover regime during low airspeeds where the lifting rotors provide the primary source of lift, and the airframe produces minimal aerodynamic effects. The aircraft is described as being in the transition regime during intermediate airspeeds where both the airframe and the lifting rotors are required to provide sufficient lift. Finally, the aircraft is described as being in the forward flight regime during high airspeeds where the airframe provides all of the necessary lift and the lifting rotors are stopped.

The operating flight regime schedule is a function of airspeed, with varying accelerating and decelerating transition speeds for hysteresis. For example the transitions from hover-to-transitional and transitional-to-forward flight regimes occur at 40 and 100 knots respectively. Conversely, the transitions from forward-to-transitional and transitional-to-hover flight regimes occur at 90 and 30 knots respectively.

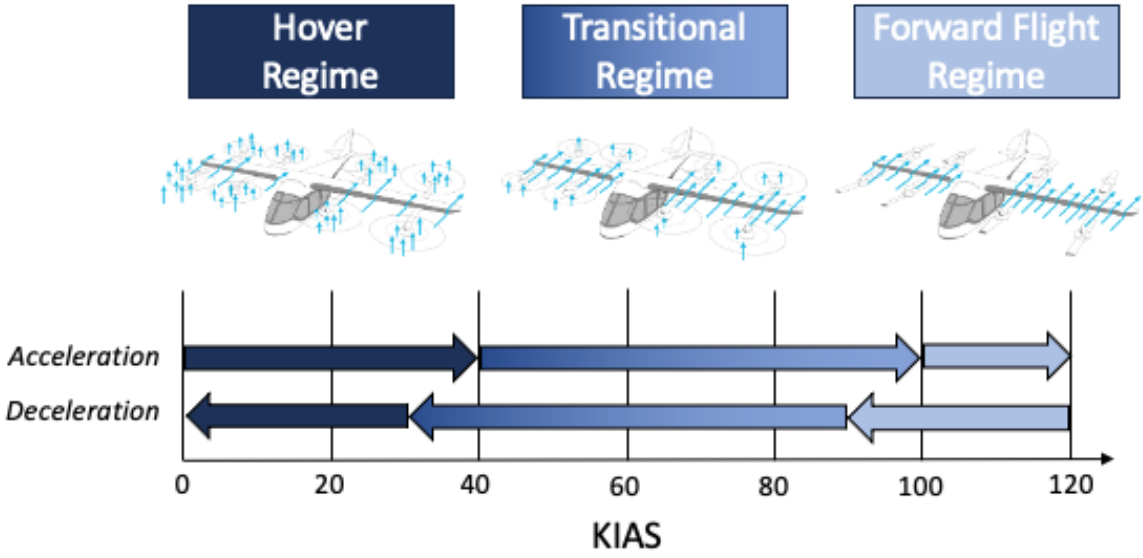

Fig. 2 Flight Regime Schedule

The control allocation schedule is illustrated in Fig. 3. In the hover regime, the lifting rotors are used collectively to produce lift for controlling the heave-axis, and differentially for maneuvering to control the pitch, roll and yaw axes. In the transitional regime, the lifting rotors are used differentially in combination with the flight control surfaces for maneuvering. Meanwhile, the lifting rotors are still used collectively to provide some lift (e.g., for angle-of-attack protection). In the forward flight regime, the lifting rotors are stopped at a neutral position and the vehicle is controlled using flight control surfaces. The pusher propeller provides forward propulsion across all flight regimes.

Control Effectors	Hover Regime	Transitional Regime	Forward Flight Regime
Collective Rotors	Heave Axis		- - -
Differential Rotors	Pitch/Roll/Yaw Axes		- - -
Flight Control Surfaces	- - -	Pitch/Roll/Yaw Axes	
Rear Propeller	Thrust Axis		

Fig. 3 Control Allocation Schedule

III. Simplified Vehicle Control System

The SVC concept was designed to simplify vehicle control by incorporating vector-based longitudinal (i.e., speed) and vertical (i.e., climb/descent) rate commands in place of pitch, heave and thrust commands. This reduces the number of axes the pilot needs to control from 5 to 4, while also allowing a control system to manage changing control strategies for the different flight regimes. This serves to simplify the pilot task by automatically changing the underlying axis of control to get a consistent vehicle response. The architecture enables inceptors to be mapped to different command response types, which describe the overall system response to pilot inputs. For a given command response type, pilot inputs generate a command that is limited by envelope protection and sent to the outer loop control system. The outer loop control system generates the necessary inner loop control commands for the current flight regime. An overview of the command system can be seen in Fig. 4. This section introduces the command response (Sec. III.A), envelope protection (Sec. III.B), outer loop control system (Sec. III.C) and inner loop control system (Sec. III.D) components that make up the SVC command system.

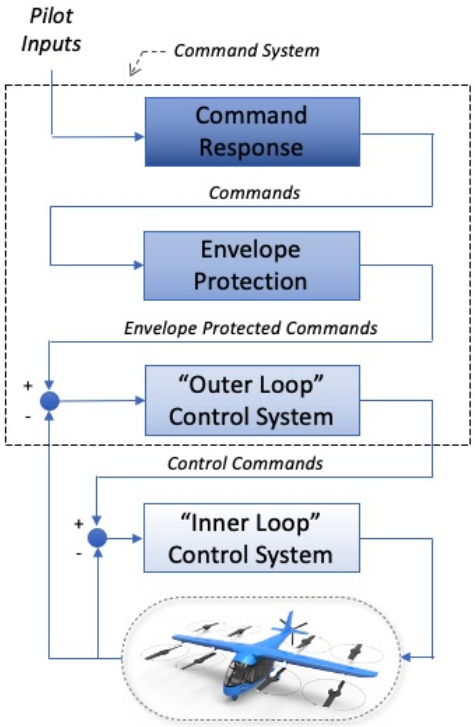

Fig. 4 Command System

The inceptor configuration utilized during this evaluation can be seen in Fig. 5. It consisted of a three-axis (longitudinal, lateral, and twist) spring-centered right stick and a single-axis spring-centered left stick. While the specific command response of each axis depends upon the flight regime, the responses can be generalized based on the resulting behavior. In general, longitudinal right stick inputs will cause the aircraft to climb or descend. Lateral right stick inputs will cause the aircraft to bank right or left. Twist right stick inputs will cause the aircraft to yaw left or right. Longitudinal left (i.e., "thrust") stick inputs will cause the aircraft to accelerate or decelerate.

There is also a hover button on the right stick that is used to arm or engage hover modes to assist the pilot in capturing and maintaining a stabilized hover position and altitude above a geographical point. Three different Assisted Hover Automation (AHA) concepts were implemented and evaluated to determine the necessary level of automation for enabling safe and efficient approach to landing maneuvers.

- The AHA-0 concept arms a "hover" mode, which engages when the groundspeed decreases below 10 knots. The "hover" mode is similar to traditional Translational Rate Command (TRC) and Rate Command Height Hold (RCHH) ADS-33 response types [18]).
- The AHA-1 concept performs a decelerating transition to the same "hover" mode.
- The AHA-2 concept performs a decelerating transition to a commanded "hover point" mode.

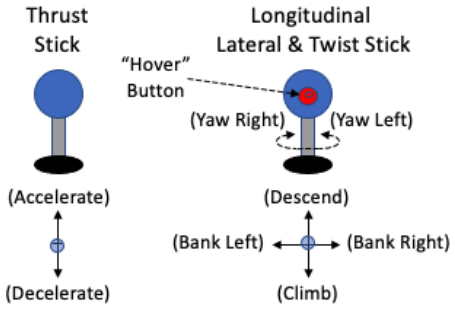

Fig. 5 Inceptor Configuration

A. Command Response

The command response system generates the appropriate commands to achieve the desired response for a given command response type. Command response types describe the overall system response to pilot inputs. The specific command response types that are active at any given moment is dependent upon the flight regime, groundspeed and hover modes. A detailed description of each command response type is provided in Appendix VI.A. In general, command response types fall under two main categories.

- <State> Command - where a constant inceptor deflection produces a constant commanded state (e.g., bank angle). Releasing the inceptor back to the neutral position results in a zero (or nominal) commanded state (e.g., wings level).
- <State 1> Command / <State 2> Hold - where a constant inceptor deflection produces a constant command for the first state (e.g., FPA rate). Releasing the inceptor back to the neutral position results in the second state (e.g., FPA angle) being maintained, even in the presence of disturbances.

1. Standard SVC Operations

The aircraft is under standard SVC operations (i.e., without assisted hover automation) when the hover button has not been pressed. An overview of the command response types under normal operations can be seen in Fig. 6. During the forward flight and transitional regimes, the right longitudinal stick commands Flight Path Angle (FPA) rate (VI.A.5), while the left stick commands acceleration/deceleration (VI.A.1). This represents a vector-based vertical command response, where the pilot does not have direct control over pitch attitude. During the transitional regime, heave is used to trim the Angle-of-Attack (AoA) for stall protection. This is described in Appendeix VI.D.1. Meanwhile, the right lateral stick commands roll rate (VI.A.12), with nominal turn coordination that can be augmented by twisting the right stick to produce sideslip commands (VI.A.13).

Inceptors		Hover Regime	Transitional Regime	Forward Flight Regime
Right Stick	Longitudinal	Vertical Accel Cmd / FPA Hold (34 KGS)	FPA Rate Cmd	
	Lateral	Bank Cmd	Roll Rate Cmd	
	Twist	Heading Rate Cmd	Sideslip Cmd	
Left Stick		Acceleration Cmd		

Fig. 6 Standard SVC Command Response Types

Since FPA becomes unreliable at slower speeds, the right longitudinal stick switches from commanding FPA rate to vertical acceleration whenever the groundspeed falls below 34 knots. This crossover takes place at the groundspeed where a flight path angle of 1 deg corresponds to a vertical speed of 1 ft/sec. However, while a constant inceptor

deflection commands a constant vertical acceleration, releasing the inceptor back to a neutral position maintains the current commanded flight path angle. This is achieved by augmenting a commanded vertical velocity target with a correction term so that flight path angle remains steady during acceleration or deceleration. This vertical acceleration command with FPA hold command response type is described in Appendix VI.A.16.

During the hover regime, the outer loop control system switches from controlling airspeed to forward groundspeed relative acceleration/deceleration, since airspeed becomes unreliable. To minimize pitch attitude changes during low speed maneuvering, acceleration/deceleration is controlled through the thrust-axis. Meanwhile the right longitudinal stick continues to command vertical acceleration (with FPA hold) through the heave-axis, and pitch-axis is nominally trimmed to a 5 degree nose up attitude to enable deceleration. This is described in Appendix VI.D.2. The right lateral stick commands bank angle (VI.A.3), instead of roll rate for stability purposes. Finally, twisting the right stick commands heading rate (VI.A.7), which can now be controlled independently of track due to the lack of sideslip considerations stemming from the vertical tail.

2. AHA-0 (Hover Armed/Engaged) Operations

Under the AHA-0 automation condition, pressing the hover button arms the "hover" mode. When "hover" is armed, the aircraft operates under the normal (non-hovering) command response types. The "hover" mode becomes engaged when the groundspeed decreases below 10 knots. The "hover" mode will remain engaged (until disengaged) and limit groundspeed to below 20 knots. An overview of the command response types under AHA-0 operations can be seen in Fig. 7. When "hover" is engaged, the right longitudinal stick commands vertical speed (VI.A.17), while the left stick commands longitudinal velocity (i.e., forward groundspeed) (VI.A.10). Similar to nominal operations in the hover regime, speed is controlled through the thrust-axis and vertical speed is controlled through the heave axis. The right lateral stick commands lateral velocity (VI.A.9), and twisting the right stick continues to command heading rate. It should be noted that one of the negative features of this inceptor configuration is that translating the aircraft's position forward and to the side is a two-handed operation.

Inceptors		Hover Engaged	Hover Armed		
			Hover Regime	Transitional Regime	Forward Flight Regime
Right Stick	Longitudinal	Vert Speed Cmd	Vertical Accel Cmd / FPA Hold (34 KGS)	FPA Rate Cmd	
	Lateral	Lat Velocity Cmd	Bank Cmd	Roll Rate Cmd	
	Twist	Heading Rate Cmd		Sideslip Cmd	
Left Stick		Lon Velocity Cmd	Acceleration Cmd		

Fig. 7 AHA-0 Command Response Types

3. AHA-1 (Hover Transition/Engaged) Operations

Under the AHA-1 automation condition, pressing the hover button engages the "hover transition" mode, which automatically commands a nominal deceleration rate ($\dot{V}_{\text{hover}}$) of 2.5 knots/sec to hover. As with AHA-0, the "hover" mode engages when the groundspeed decreases below 10 knots. An overview of the command response types under AHA-1 operations can be seen in Fig. 8.

During "hover transition", in addition to automatically decelerating, AHA-1 also decrabs the aircraft (e.g., in the presence of a crosswind). This has the advantage of reducing the primary axes the pilot needs to control (over standard SVC operations) from 4 to 2. To improve handling qualities while decelerating with a potential sideslip, AHA-1 also transitions to a vector-based lateral command response, where the pilot does not have direct control over bank attitude. The left stick continues to command acceleration/deceleration (VI.A.1), with the exception of an input bias resulting in the nominal deceleration rate that can be overridden by the pilot. The right twist stick commands crab (instead of sideslip) to automatically decrab the aircraft (VI.A.4). The right lateral stick commands track angle rate with track

Inceptors		Hover Engaged	Hover Transition		
			Hover Regime	Transitional Regime	Forward Flight Regime
Right Stick	Longitudinal	Vert Speed Cmd	Vert Accel Cmd / FPA Hold	34 KGS	FPA Rate Cmd / FPA Hold
	Lateral	Lat Velocity Cmd	Lat Accel Cmd / Track Hold	34 KGS	Track Rate Cmd / Track Hold
	Twist	Heading Rate Cmd			Crab Cmd
Left Stick		Lon Velocity Cmd	Acceleration Cmd		

Fig. 8 AHA-1 Command Response Types

hold (instead of roll rate) (VI.A.15), until the groundspeed falls below 34 knots and it switches to commanding lateral acceleration with track hold. This is achieved by augmenting the commanded lateral velocity target with a correction term so that track angle remains steady during acceleration or deceleration. This is described in Appendix VI.A.8. Finally, the right longitudinal stick behaves similar to nominal operations, except that the response type incorporates a slightly slower FPA rate command with FPA hold response type (verses FPA rate command) to more accurately track the desired glidepath in the presence of sideslip (VI.A.6). When "hover" is engaged, the command response types are the same as AHA-0.

To assist the pilot in determining when to initiate "hover transition" and managing the dissipation of kinetic energy during deceleration, a predicted hover point is computed and displayed to the pilot (on a map display, described later in IV.B.2 and seen in Fig. 17). Prior to "hover transition", the predicted hover point is computed based on a nominal deceleration rate ($\dot{V}_{\text{hover}}$) and the current track angle (χ). The predicted hover point is calculated as follows:

$$\Delta t_{\text{hov}} = \frac{V_{\text{gnd}}}{\dot{V}_{\text{hover}}} \tag{1}$$

$$d_{\text{hov}} = \frac{1}{2} V_{\text{gnd}} \Delta t_{\text{hov}} \tag{2}$$

$$\text{lat}_{\text{hov}} = \text{lat} + d_{\text{hov}} \cdot \frac{\cos\chi}{R_e} \cdot \frac{180}{\pi} \tag{3}$$

$$\text{lon}_{\text{hov}} = \text{lon} + d_{\text{hov}} \cdot \frac{\sin\chi}{R_e \cos\text{lat}} \cdot \frac{180}{\pi} \tag{4}$$

During "hover transition", the predicted hover point is computed the same, except that the current track angle is replaced by the commanded track angle (χ_{cmd}):

$$\text{lat}_{\text{hov}} = \text{lat} + \text{d}_{\text{hov}} \cdot \frac{\cos\chi_{\text{cmd}}}{R_e} \cdot \frac{180}{\pi} \tag{5}$$

$$\text{lon}_{\text{hov}} = \text{lon} + \text{d}_{\text{hov}} \cdot \frac{\sin\chi_{\text{cmd}}}{R_e \cos\text{lat}} \cdot \frac{180}{\pi} \tag{6}$$

During "hover engaged", the predicted hover point is computed based on ground speed components:

$$\dot{X} = \frac{1}{\tau_{\text{TRC}}} V_{X_{\text{cmd}}} - V_{\text{gnd}_X} \tag{7}$$

$$\dot{Y} = \frac{1}{\tau_{\text{TRC}}} V_{Y_{\text{cmd}}} - V_{\text{gnd}_Y} \tag{8}$$

and the Translational Rate Command (TRC) outer loop control system (VI.E.12) time constant (τ_{TRC}):

$$\Delta X = V_{\text{gnd}_X} \cdot \tau_{\text{TRC}} + \dot{X} \cdot \tau_{\text{TRC}} \tag{9}$$

$$\Delta Y = V_{\text{gnd}_Y} \cdot \tau_{\text{TRC}} + \dot{Y} \cdot \tau_{\text{TRC}} \tag{10}$$

which are then used to calculate updated hover point prediction coordinates:

$$\Delta N = \Delta X \cos\psi - \Delta Y \sin\psi \tag{11}$$

$$\Delta E = \Delta X \sin\psi + \Delta Y \cos\psi \tag{12}$$

$$\text{lat}_{\text{hov}} = \text{lat} + \frac{\Delta N}{R_e}\frac{180}{\pi} \tag{13}$$

$$\text{lon}_{\text{hov}} = \text{lon} + \frac{\Delta E}{R_e \cos\text{lat}}\frac{180}{\pi} \tag{14}$$

4. AHA-2 (Hover Point Transition/Engaged) Operations

Under the AHA-2 automation condition, pressing the hover button engages the "hover point transition" mode, which automatically decelerates while flying to a commanded hover point. This point is initialized at or near the predicted hover point that is computed in Eq. (3)–(4), and displayed to the pilot (on a map display, described later in IV.B.3 and seen in Fig. 18). Left stick and right lateral stick commands move the location of the commanded hover point longitudinally and laterally with respect to the heading of the vehicle. When these inceptors are in a neutral position, the commanded hover point will remain stationary. The "hover point" mode engages upon hover point capture (see Eq. (15)). An overview of the command response types under AHA-2 operations can be seen in Fig. 9.

Inceptors		Hover Point Engaged	Hover Point Transition		
			Hover Regime	Transitional Regime	Forward Flight Regime
Right Stick	Longitudinal	Vert Speed Cmd	Vert Accel Cmd FPA Hold	34 KGS	FPA Rate Cmd FPA Hold
	Lateral	Lat Velocity Cmd Lat Position Hold		34 KGS	Track Rate Command Lat Position Hold
	Twist	Heading Rate Cmd			Crab Cmd
Left Stick		Lon Velocity Cmd Lon Position Hold	Acceleration Cmd Lon Position Hold		

Fig. 9 AHA-2 Command Response Types

The command response types are similar to AHA-1, except that left stick and right lateral stick response types incorporate a longitudinal and lateral position hold respectively. During "hover point transition", the left stick commands acceleration with longitudinal position hold (VI.A.2). The right lateral stick commands track angle rate with lateral position hold (VI.A.14, until the groundspeed decreases below 34 knots and it switches to command lateral velocity with lateral position hold (VI.A.11). This has the advantage (over AHA-1) of reducing the primary axes the pilot needs to control from 2 to 1 (i.e., allowing the pilot to focus on altitude management while the aircraft is decelerating and decrabbing while flying along a vector to the hover point). During "hover point engaged", the left stick commands longitudinal velocity with longitudinal position hold (VI.A.11) and the right lateral stick commands lateral velocity with lateral position hold (VI.A.11).

To assist the pilot in determining when to initiate "hover point transition", a predicted hover point is computed using Eq. (3)–(4), and displayed to the pilot (on a map display). If the hover button is pressed when the predicted hover point is near a helipad, then the commanded hover point (lat_{cmd}, lon_{cmd}) is initialized to the location of that helipad. Otherwise, the commanded hover point is initialized to the predicted hover point.

As with AHA-0 and AHA-1, the "hover point" mode engages when the groundspeed decreases below 10 knots. However, below 20 knots, the mode can also engage upon hover point capture. This occurs when the commanded ground speed $V_{\text{gnd}_{\text{cmd}}}$, corresponding to the "hover point engaged" outer loop control laws, becomes less than the measured groundspeed V_{gnd}:

$$V_{\text{gnd}_{\text{cmd}}} < \min\left(V_{\text{gnd}}, 20 \text{ kts}\right) \tag{15}$$

The commanded ground speed is computed as a function of the distance from the commanded hover point and the Position Rate Command / Position Hold (VI.A.11) time constants (τ_{pos}):

$$\Delta N = (\text{lat}_{\text{cmd}} - \text{lat}) \cdot \frac{\pi}{180} \cdot R_e \tag{16}$$

$$\Delta E = (\text{lon}_{\text{cmd}} - \text{lon}) \cdot \frac{\pi}{180} \cdot R_e \cos \text{lat} \tag{17}$$

$$\Delta X = \Delta N \cos\psi + \Delta E \sin\psi \tag{18}$$

$$\Delta Y = \Delta E \cos\psi - \Delta N \sin\psi \tag{19}$$

$$V_{X_{\text{cmd}}} = \frac{1}{\tau_{\text{pos}}} \Delta X \tag{20}$$

$$V_{Y_{\text{cmd}}} = \frac{1}{\tau_{\text{pos}}} \Delta Y \tag{21}$$

$$V_{\text{gnd}_{\text{cmd}}} = \sqrt{V_{X_{\text{cmd}}}^2 + V_{Y_{\text{cmd}}}^2} \tag{22}$$

B. Envelope Protection

Envelope protection ensures that the aircraft response to pilot inputs will stay within safe operating limits. While this includes the maximum operating limit speed, stall protection may not apply as long as the vehicle remains VTOL capable. Furthermore, since the SVC system changes the nature of the aircraft's response to pilot inputs, the envelope protection system also has to change accordingly. Conventional envelope protection concepts (e.g., pitch attitude and angle-of-attack protection) get altered or replaced by higher-level command protection (e.g., flight path angle rate command protection). During the transition flight regime, the aircraft flight envelope is reduced and energy trade offs may need to be made to maintain speed (or deceleration/acceleration) and descent/climb rates. Some slight authority is given to path over speed (as seen in Appendix VI.B.4). A detailed description of each envelope limit is provided in Appendices VI.B and VI.C. In general, the purpose of these envelope limits fall under two main categories: command protection and envelope awareness.

1. Command Protection

The purpose of command protection is to apply envelope limits to the commands generated by the command response types, before they are sent to the outer loop control systems. The calculation of these envelope limits needs to incorporate the time constants of the outer loop control laws to enable the smooth capture of the corresponding operating limits. In some cases, kinetic and potential energy trade-offs need to be incorporated into higher-level envelope limit calculations, as is the case with acceleration/deceleration and flight path angle rate command limits. A detailed description of each envelope limit for command protection is provided in Appendix VI.B.

2. Envelope Awareness

Several of the envelope limits are also displayed to the pilot (on a primary flight display). This was intended to enhance situational awareness when the aircraft is approaching or has encountered envelope limits. In many cases (e.g., bank and sideslip angle limits), the command protection limits are used directly to drive these display elements. In other cases (e.g., involving the saturation of the rear propeller), command protection limits may not be available for displaying the desired display elements (e.g., achievable airspeed limits). In these cases, a predicted envelope limit may need to be computed (e.g., based on available thrust capability). A detailed description of each envelope limit for awareness purposes is provided in Appendix VI.C.

C. Outer Loop Control System

For a given command response type, pilot inputs generate command response outputs for the outer loop control system. Additional commands are generated by the automatic trim system, described in Appendix VI.D. The outer loop control system is responsible for mapping the outer loop responses to the necessary inputs for the inner loop control system, which is dependent upon the flight regime. Fig. 10 shows the outer loop control architecture, specifically how the individual automatic trim and outer loop control systems (rectangles) are interconnected and connected to the inner loop control systems (ovals). Since some command response types are scheduled with respect to flight regime and

others are dependent upon groundspeed, the path of the interconnected control systems may differ with wind conditions. Detailed descriptions of the outer loop control systems are all explained in Appendix VI.E.

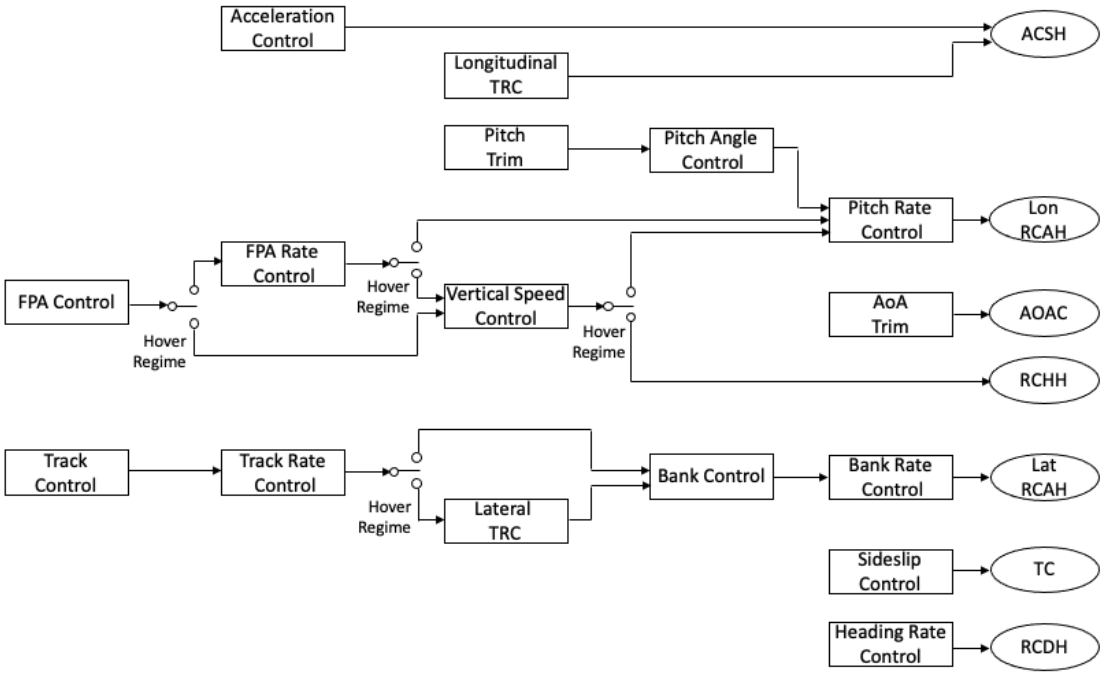

Fig. 10 Outer Loop Control Architecture

D. Inner Loop Control System

A Nonlinear Dynamic Inversion (NDI) based flight control system is used to provide inner loop stability and control augmentation [19, 20], which enables rapid integration and evaluation of new vehicle models. The integration process begins by determining the control allocation and mixing strategies for all of the control effectors, as seen in Fig. 3. Then the desired inner loop control modes (corresponding to ADS-33 response types [18]) are determined. These control modes were determined with consideration to vehicle operation and performance. As a result, control modes are scheduled automatically as a function of flight regime. The schedule of the control modes used in this evaluation are displayed in Fig. 11. Analysis of the open-loop dynamics of the vehicle is used to specify the reference model and error controller gains that correspond to the control system for each control mode. These mode specific controllers generate acceleration commands that are used to compute control effector commands through model inversion. An overview of the controller architecture can be seen in Fig. 12.

While most of these control modes have heritage in ADS-33 [18], some new ones were added for enabling simplified operations. Pitch, roll and yaw control modes provide rotational stability and control augmentation. The rotational control modes consisted of Rate Command Attitude Hold (RCAH) for pitch and roll control, and Rate Command Direction Hold (RCDH) and Turn Coordination (TC) for yaw control. For the yaw modes, RCDH provides yaw control at lower speeds (i.e., in the hover regime). Once aerodynamic effects take effect (i.e., in the transitional and forward flight regimes), sideslip considerations necessitate the use of TC. Translational modes include Rate Command Height Hold (RCHH) and Angle-of-Attack Command (AOAC) for heave, and Acceleration Command Speed Hold (ACSH) for thrust. When at lower speeds, the collective lifting rotors can provide direct altitude control through RCHH. As aerodynamic effects influence vehicle behavior, AOAC supports an angle-of-attack protection system. ACSH allows for simplified speed control (i.e., the magnitude of the velocity vector). More technical details on the different aforementioned inner loop control modes are given in Appendix VI.F.

Control Axes	Hover Regime	Transitional Regime	Forward Flight Regime
Heave Axis	Rate Command Height Hold (RCHH)	Angle-of-Attack Command (AOAC)	- - -
Pitch and Roll Axes	Rate Command Attitude Hold (RCAH)		
Yaw Axis	Rate Command Direction Hold (RCDH)	Turn Coordination (TC)	
Thrust Axis	Acceleration Command Speed Hold (ACSH)		

Fig. 11 Control Mode Schedule

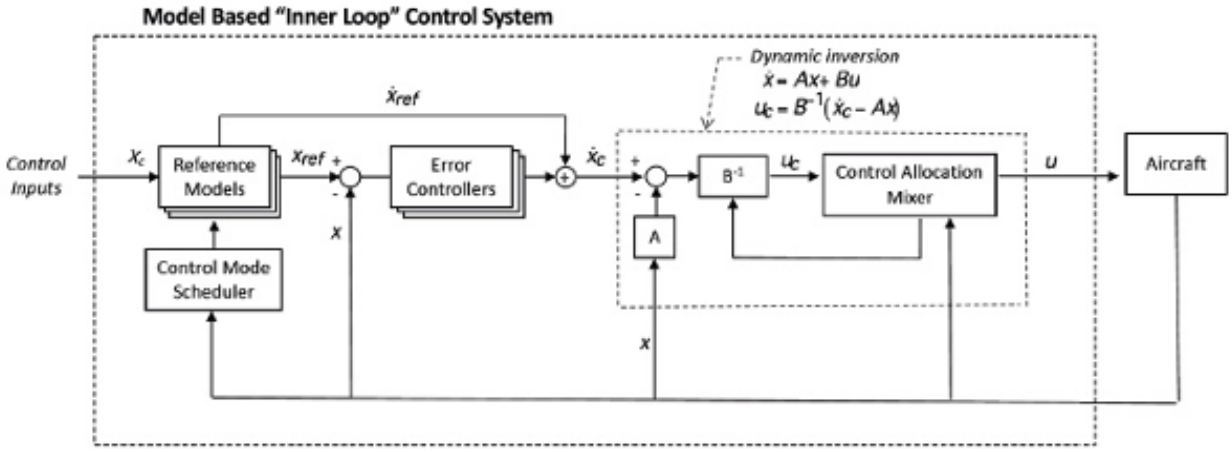

Fig. 12 Inner Loop Control System

IV. Simulation Tests

The SVC concept was implemented and tested in a high fidelity simulation environment. The tests consisted of a research pilot flying approach to landing maneuvers under each of the Assistive Hover Automation (AHA) conditions. This section provides an overview of the simulation environment (IV.A), a description of the tests that were performed (IV.B), and the corresponding results using AHA-0 (IV.C), AHA-1 (IV.D) and AHA-2 (IV.E).

A. Test Environment

The LPC model (II) and SVC system (III) were integrated into the Aerospace Cognitive Engineering Lab – Rapid Automation Test Environment (ACEL-RATE) simulator at NASA Ames. This fixed-based simulator, shown in Fig. 13), is used for testing, development and validation. It consists of wide-view outside visual display, three primary displays, two chin-window displays, and reconfigurable cockpit hardware (currently in a two stick inceptor configuration, as defined in Fig. 5). The Out-the-Window is a 200-degree field of view screen which runs a customized visual database built in RSI [21].

(a) Simulator facility (b) Pilot station

Fig. 13 ACEL-RATE simulator

The flight displays consist of a Primary Flight Display, a Navigation (Map) Display, and a System Health Display. The Primary Flight Display, shown in Fig. 14, provides attitude, altitude, and speed information as well as glidepath and final approach course deviations overlaid on a synthetic/enhanced vision background. A dual-cue flight director is displayed as magenta crosshairs. The envelope limits described in III.B.2 for airspeed, vertical speed, bank and sideslip, are also displayed on the PFD. The red bars show command limits while the amber/yellow bars show estimated margins to saturation. As described in III.B, in this amber region, the aircraft will need to trade climb/descent rates with decreasing/increasing airspeed.

The Navigation (Map) Display, shown in Fig. 15, provides a top down view of ground reference information against a black background. The map displays active flight plan information, including the reference trajectory shown in magenta, waypoint indicators with speed and altitude constraints shown in green, and the target landing site indicated by a cyan circle. In the forward flight and transitional regimes, a white segmented position trend vector is visible, extending from the aircraft. Each line segment predicts the position at the end of 30, 60 and 90 seconds (based on bank angle and ground speed). Both automatic and manual zoom functionality are provided to the pilot to change the map scale. The pilot also has an option to toggle the map to a 90-deg (belly) or 45-deg (chin) camera view, which can be useful to obtain a better view of the landing site.

The System Health display, shown in Fig. 16, provides information on actuator or control saturation as well as battery usage. For the lifting and pusher propellers, blade pitch limits are shown as percentages. For each of the control axes (roll, pitch, yaw, heave, thrust), control authority limits are shown. These represent either control surface deflection limits and/or a percentage of rotor authority used allocated to that axis. The battery time remaining is calculated based on long range cruise consumption (and therefore decreases faster than real-time while in hover).

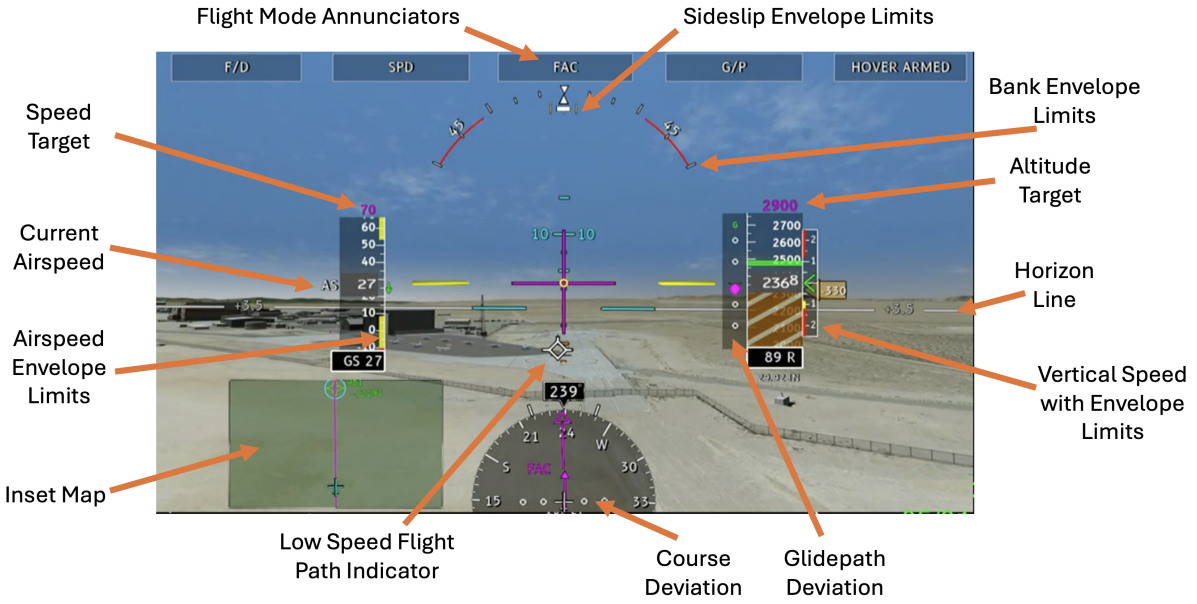

Fig. 14 Primary Flight Display

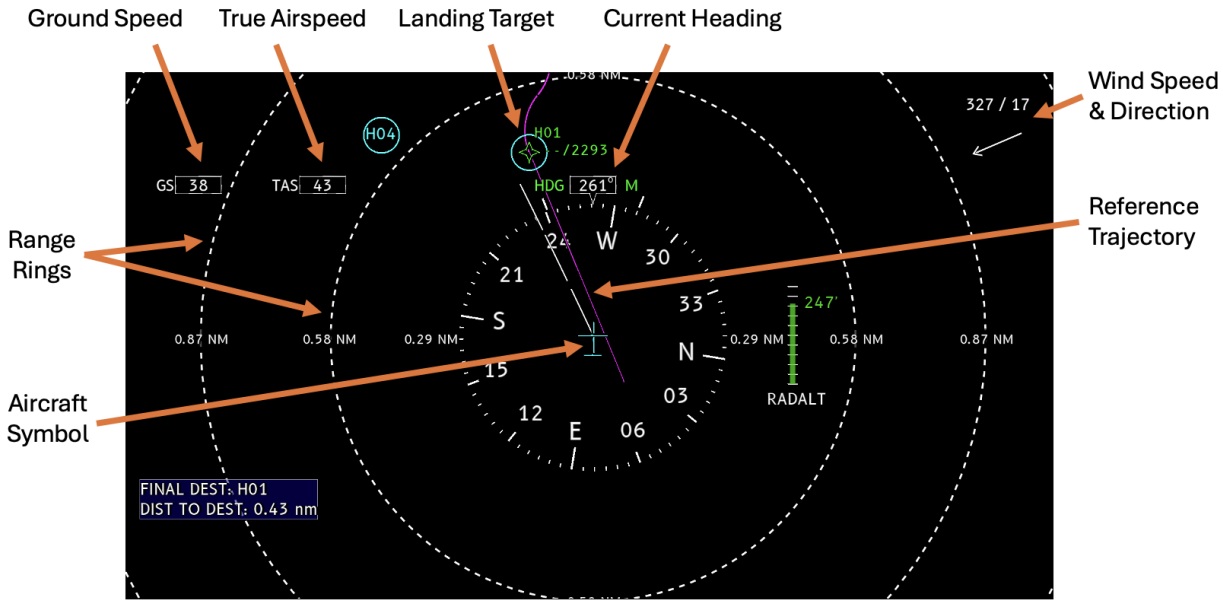

Fig. 15 Navigation Display

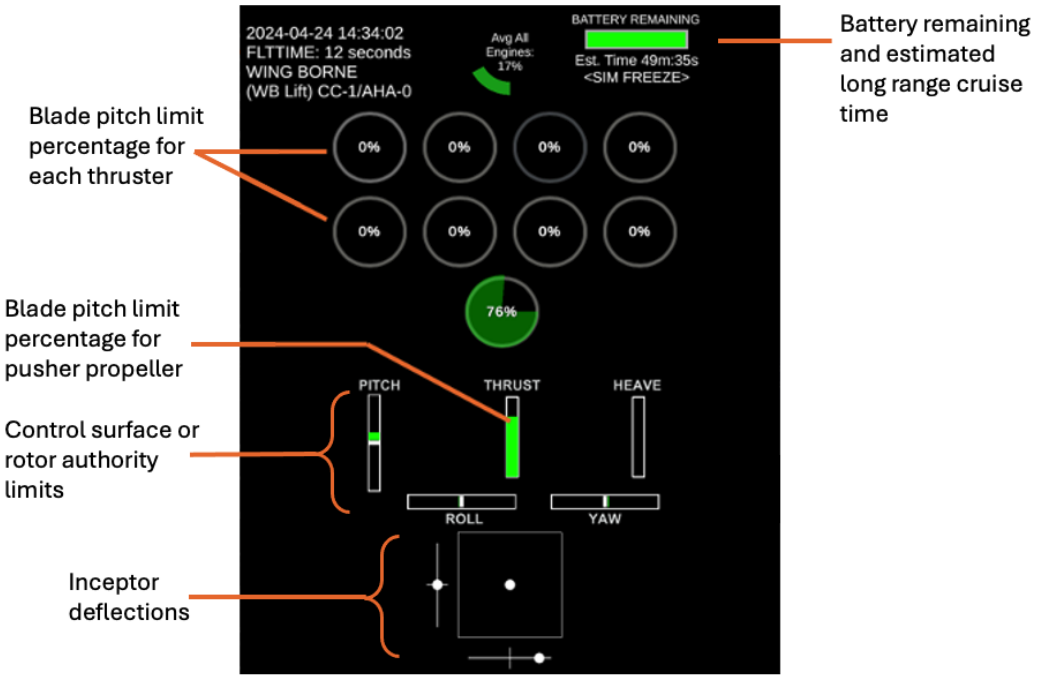

Fig. 16 System Health Display

B. Test Description

The tests were flown on a 6 degree glidepath at an initial altitude of 500 feet above ground level, with a 17 knot crosswind. For energy efficiency, an initial airspeed of 70 knots was maintained, until initiating a nominal 2.5 knot per second deceleration rate to come to a stabilized hover over the helipad. The pilot was asked to touchdown inside of 5' (preferably) and 10' rings painted on the helipad landing site and to align with the approach course prior to touchdown. The maneuver is completed upon touchdown. The research pilot was trained on each of the AHA conditions. For these tests, the pilot was instructed to try to utilize the automation features that each AHA condition provided to the extent possible.

1. AHA-0 Test Description

During AHA-0 tests, the pilot determines when to begin the deceleration and continues to manage the deceleration rate to the helipad. Pressing the hover button arms the hover mode. The hover mode engages when the groundspeed decreases below 10 knots. As a result of decelerating in crosswind, the pilot may also need to augment lateral and directional control to maintain track in the presence of crab and/or sideslip angles.

2. AHA-1 Test Description

During AHA-1 tests, the pilot was instructed to utilize the proximity of the predicted hover point relative to the helipad symbol to determine when to press the hover button (as shown in Figure 17). After pressing the hover button, the velocity vector line to the predicted hover point changes from white to green, since the command response type changes to a vector-based (track) command (as the aircraft automatically decrabs). During the automatic deceleration, the pilot may need to augment the left stick to adjust the location of the predicted hover point if it drifts away from the helipad symbol.

3. AHA-2 Test Description

During AHA-2 tests, the pilot was instructed to utilize the proximity of the predicted hover point relative to the helipad symbol to determine when to press the hover button (as shown in Figure 18). After pressing the hover button, the white predicted hover point latches to the helipad and becomes a green commanded hover point. The velocity vector

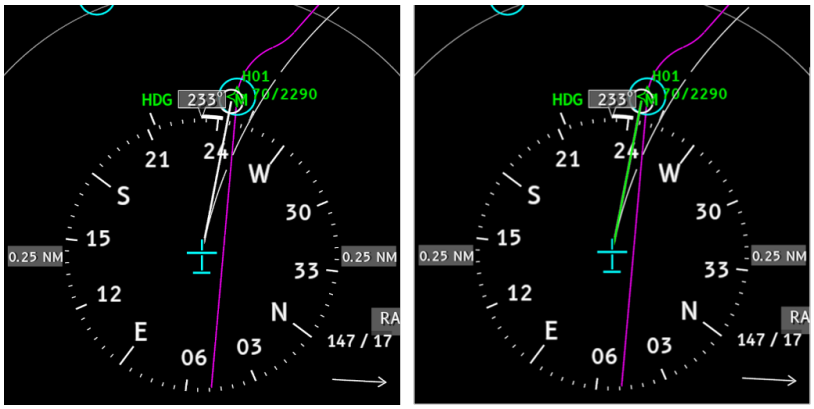

(a) Before pressing the hover button (b) After pressing the hover button

Fig. 17 AHA-1 predicted hover point

line also changes from white to green, since the command response type changes to fly to the commanded hover point (as the aircraft automatically decrabs).

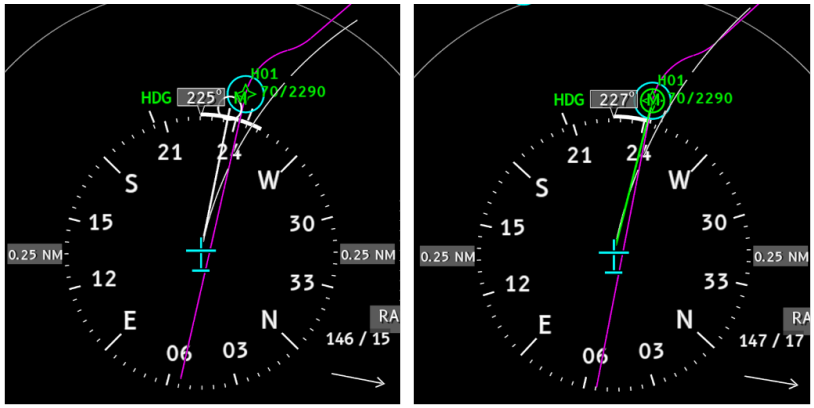

(a) Before pressing the hover button (b) After pressing the hover button

Fig. 18 AHA-2 predicted/commanded hover point

C. AHA-0 Test Results

As described in Sec. III.A.2, this concept is the lowest automation level and does not include automatic deceleration or decrab maneuvers. The hover button simply arms the hover mode, which eventually engages when the groundspeed decreases below 10 kts.

1. Trajectory

Fig. 19 shows the full trajectory for AHA-0, with Fig. 19(a) the altitude profile of altitude above ground level along the reference groundtrack distance down to the bottom of descent and Fig. 19(b) the ground track together with a vector arrow showing the wind direction. The landing point is at the origin of the ground track figure. The dashed lines show the reference path down to hover height. Tracking the reference path works well at higher speeds, but becomes more difficult while manually decelerating to hover. This especially shows below 150 ft altitude in Fig. 19(a). More details on the ground track during manual hover transition are shown in Sec. IV.C.3.

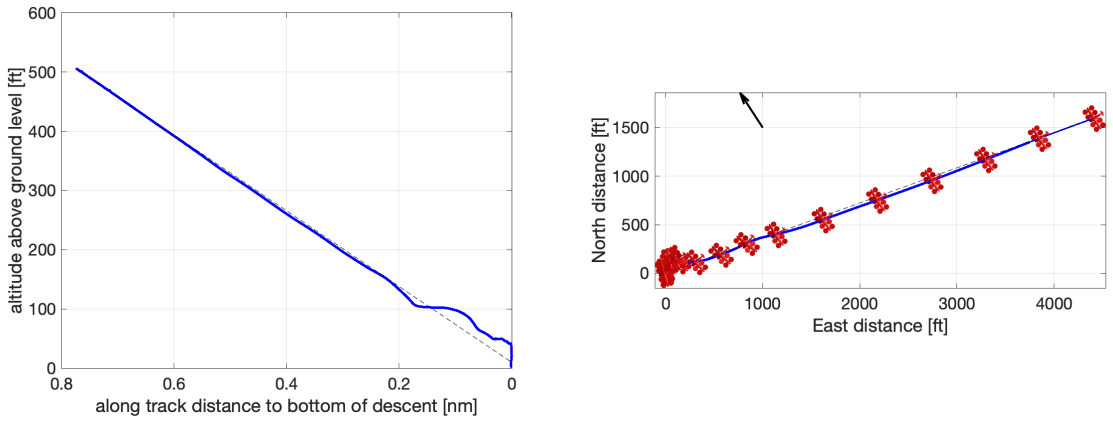

(a) Altitude profile

(b) Ground track

Fig. 19 Full run trajectory for AHA-0

2. Deceleration characteristics

Fig. 20 shows the deceleration profile during this maneuver. Fig. 20(a) shows the entire run, and Fig. 20(b) focuses on the final phase of the maneuver which covers the last 120 ft along track distance until touchdown. The various plots from top to bottom show ground speed, deceleration (command and response) and thrust stick activity. Various linewidths indicate out-of-hover flight (thinnest line before 0.65 nm distance), hover armed (medium linewidth after 0.65 nm distance) and hover engaged (largest linewidth below 10 kts (equals 16 ft/s) groundspeed). The pressing of the hover button (to arm the hover mode) is marked by the red vertical dashed line in the thrust stick activity plot. Fig. 20(a) confirms that no automatic deceleration happens by arming hover in AHA-0. The vehicle decelerates by pulling back the thrust stick manually just after 0.3 nm along track distance. Full thrust stick authority is used in portions of the deceleration phase. Minor adjustments forward are given in the hover engaged phase to move the vehicle forward to the landing zone. Anticipating the location where the vehicle will come to a standstill ahead of time in the deceleration phase is not straightforward due to the lack of predictive information. At the very end, the vehicle drifts laterally over and beyond the landing target marker, as best seen in Fig. 23, which requires some minor corrections that show up inside the 10 ft along track distance range in Fig. 20(b).

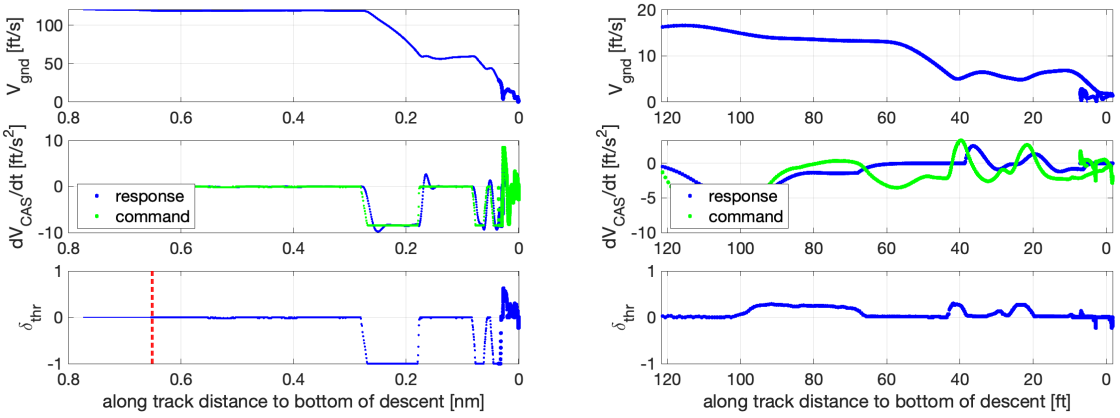

(a) Full run

(b) Final phase

Fig. 20 Deceleration characteristics for AHA-0

3. Decrab characteristics

The decrab maneuver is illustrated in Fig. 21. Fig. 21(a) shows both sideslip angle β (direction of airspeed vector wrt vehicle nose) and crab angle $\psi_{\text{crab}} = \psi - \chi$ (direction of ground speed vector wrt vehicle nose), together with the yaw rate (command and response) as well as stick twist. Since there is no automatic decrab maneuver in AHA-0, the slip angle remains quasi-steady while the crab angle drifts off during manual deceleration. This results in the vehicle drifting downwind off track, as illustrated in Fig. 21(b). The pilot executes some stick twist action after hover engages (indicated by the vertical dash dotted line in the stick twist graph) to bring the crab angle to zero.

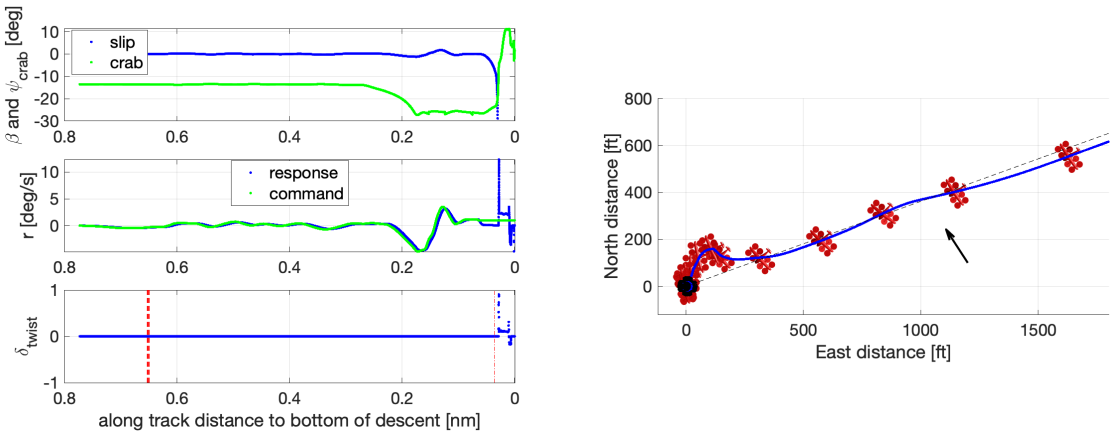

(a) Slip versus crab angle

(b) Ground track hover armed

Fig. 21 Decrab characteristics for AHA-0

4. Hover characteristics

Fig. 22 shows ground track in Fig. 22(a) and stick activity in Fig. 22(b) for the entire hover engaged phase. Early in the hover engaged phase, the vehicle drifts off downwind from the reference track and the pilot yaws as well for aligning the heading with the helipad, requiring significant pilot compensation in three axes – forward, sideways and yaw – as illustrated in Fig. 22(b). Also longitudinal stick activity follows at the very end, but only for touching down on the helipad.

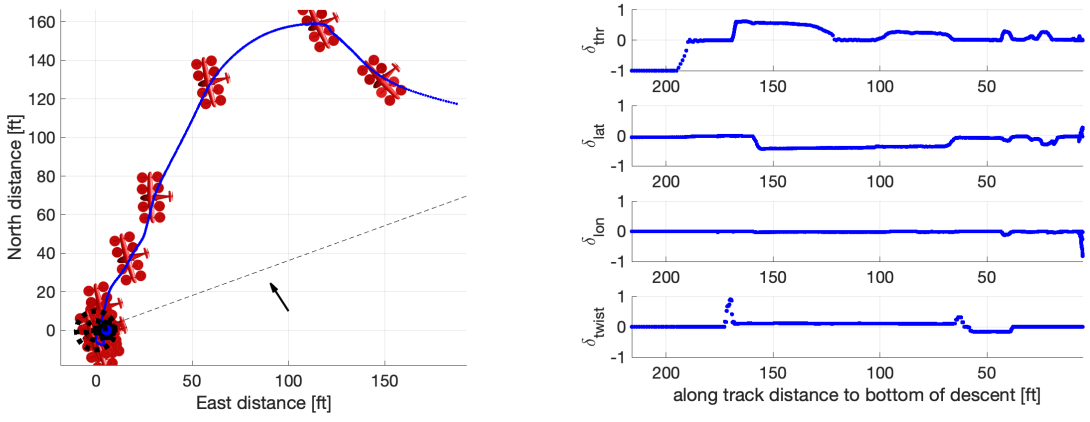

(a) Ground track

(b) Stick activity

Fig. 22 Hover characteristics for AHA-0

Fig. 23 zooms in on the ground track around the helipad, and illustrates the difficulties to pinpoint the vehicle close to the center of the circles in crosswind conditions, resulting in a few sideways overshoots.

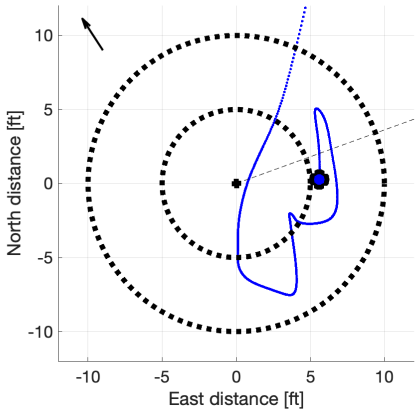

Fig. 23 Ground track around the helipad for AHA-0

D. AHA-1 Test Results

As described in Sec. III.A.3, this concept is the intermediate automation level and includes automatic deceleration with decrab maneuvers. The transition engages by pressing the hover button and results in a nominal deceleration rate (that can be overridden by the pilot). Hover mode engages when the groundspeed decreases below 10 kts, as with AHA-0. A key feature of the AHA-1 automation condition is a predicted hover point that is displayed to the pilot on a map display (as seen in Fig. 17), which assists the pilot in determining when to initiate hover transition and also to make corrections during the transition. Details about the predicted hover point calculations are given in Sec. III.A.3.

1. Trajectory

Fig. 24 shows the full trajectory for AHA-1 in a similar fashion as was done for AHA-0 in Fig. 19. Tracking the reference path works well at all speeds with this higher automation level, even while decelerating in the hover transition. The most significant contrast with AHA-0 shows below 150 ft altitude by comparing Fig. 24(a) and Fig. 19(a). More details on the ground track during automatic hover transition are shown in Sec. IV.D.3.

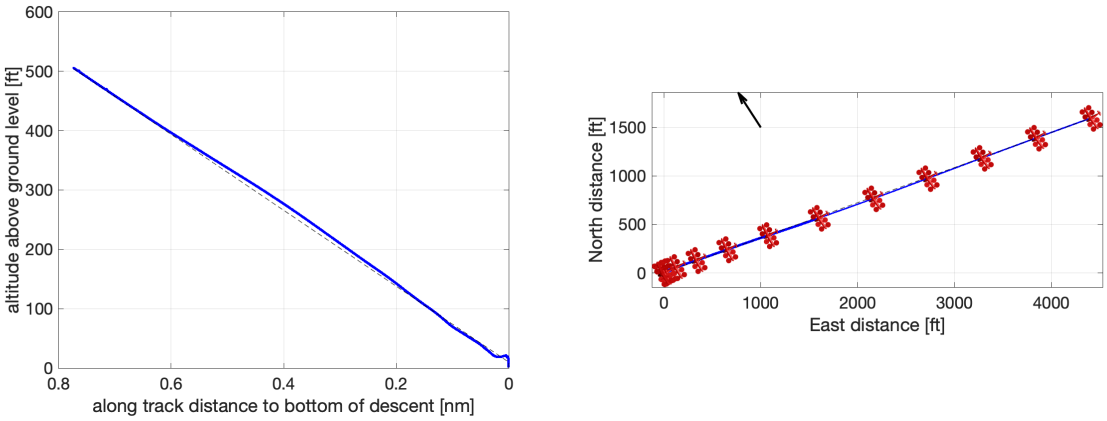

(a) Altitude profile

(b) Ground track

Fig. 24 Full run trajectory for AHA-1

2. Deceleration characteristics

Fig. 25 shows the deceleration profile during this maneuver in a similar fashion as was done for AHA-0 in Fig. 20. The pressing of the hover button (to engage hover transition) is marked by the red vertical dashed line in the thrust stick activity plot around 0.3 nm along track distance. Fig. 25(a) shows how the automatic deceleration is activated by engaging the hover transition in AHA-1. From that moment onward, the vehicle decelerates automatically around 4 ft/s^2 (equal to 2.5 kts/s) as dictated by $\dot{V}_{\text{hover}}$ (explained in detail in Sec. III.A.3) without pulling back the thrust stick manually. The thrust stick can be used to override the automatic deceleration rate. Minor thrust stick adjustments are given forward and backward in the hover engaged phase to move the vehicle forward to the landing zone, as shown in Fig. 25(b).

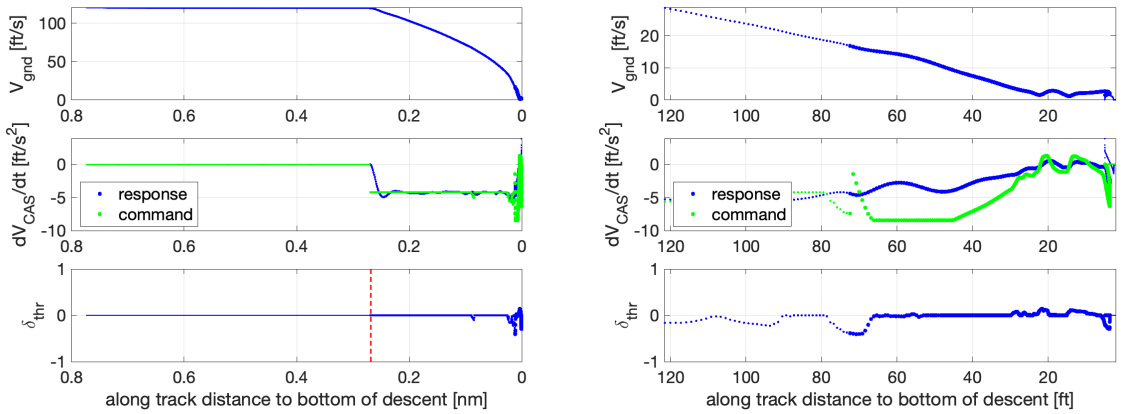

(a) Full run (b) Final phase

Fig. 25 Deceleration characteristics for AHA-1

3. Decrab characteristics

The automatic decrab maneuver is illustrated in Fig. 26. Fig. 26(a) shows how sideslip angle β and crab angle ψ_{crab} trade off between each other. The vehicle moves gradually from a pure crab angle and no sideslip flight condition to a nonzero sideslip and minimal crab angle configuration. This trade off starts when the hover transition is engaged. Fig. 26(a) also shows yaw rate (command and response) as well as stick twist. The vertical red dashed line on the stick twist plot shows when hover transition is initiated. Thanks to the automatic decrab mode, no stick twist is necessary for this maneuver. One can also see that the vehicle remains well on track during the transition, as illustrated in Fig. 26(b). This is a major difference compared to Fig. 21(b) for AHA-0.

4. Hover characteristics

Fig. 27 shows ground track in Fig. 27(a) and stick activity in Fig. 27(b) for the entire hover engaged phase. The ground track shows the actual position of the vehicle as well as the location of the hover predictor. As it is a hover predictor, it tends to drift off a bit during the transition maneuver, especially moving towards the vehicle indicating a tendency to stop short, which can then be compensated for by the pilot by moving the predictor forwards by means of the inceptors. In the course of the hover engaged phase, the vehicle drifts off only minimally from the reference track and doesn't yaw at all, requiring significant less pilot compensation in only two axes, forward and sideways, as illustrated in Fig. 27(b). This is in sharp contrast to the three axes control task in hover for AHA-0 as shown in Fig. 22(b). Longitudinal stick activity follows only at the end, for touching down on the helipad, which was similar for AHA-0 in Sec. IV.C.4.

Fig. 28 zooms in on the ground track around the helipad, shows again both actual ground track and hover predictor, and illustrates the ease to pinpoint the vehicle close to the center of the circles, even in crosswind conditions.

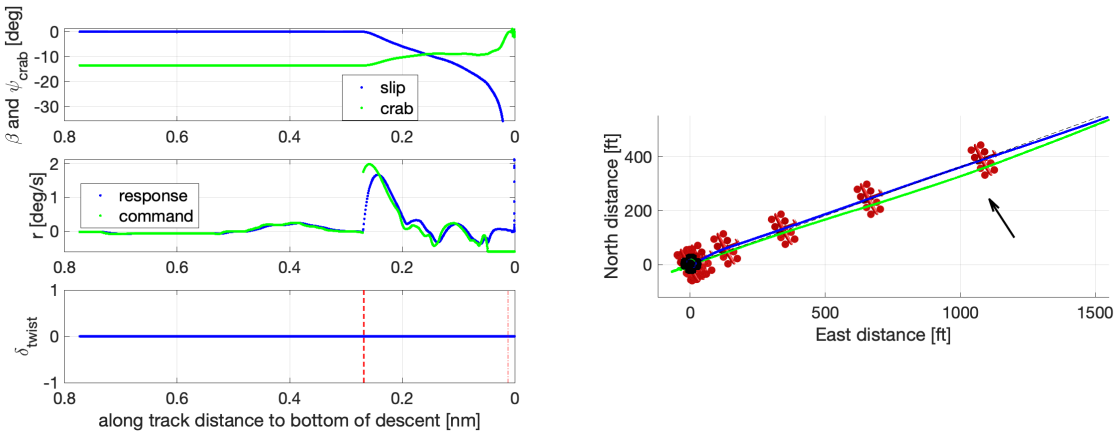

(a) Slip versus crab angle

(b) Ground track hover transition

Fig. 26 Decrab characteristics for AHA-1

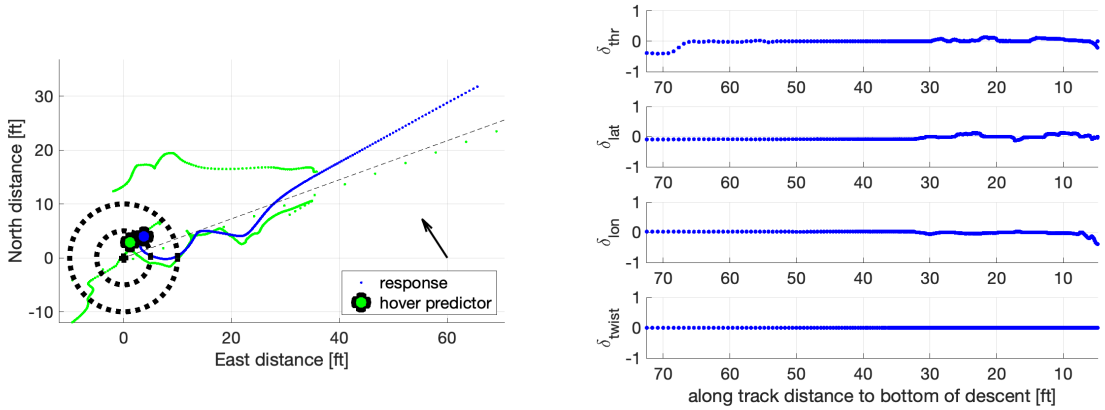

(a) Ground track

(b) Stick activity

Fig. 27 Hover characteristics for AHA-1

E. AHA-2 Test Results

As described in Sec. III.A.4, this concept is the highest automation level and includes automatic deceleration with decrab maneuvers, similar to AHA-1. The key differentiating feature of the AHA-2 automation condition, compared to AHA-1, is the implementation of a commanded hover point that is computed (similarly like the predicted hover point for AHA-1) before hover transition and displayed to the pilot on a map display, which assists the pilot in determining when to initiate hover point transition. Once hover point transition is engaged by means of the hover button, the hover point location is anchored on the map, latches the landing site center if pressed when the prediction is sufficiently close, and effectively becomes the target location where the vehicle will end up in hover point mode at the end of the hover point transition. It is still possible for the pilot to make adjustments to the hover target location during transition and in hover. Details about how the target hover point is calculated and captured are given in Sec. III.A.4.

The trajectory and decrab characteristics are not discussed in depth here for AHA-2 since these results are highly similar to the ones for the AHA-1 concept discussed in Sec. IV.D.1 and IV.D.3. However, deceleration characteristics in Sec. IV.E.1 and hover characteristics in Sec. IV.E.2 highlight important differences that are introduced by concept AHA-2 compared to AHA-1.

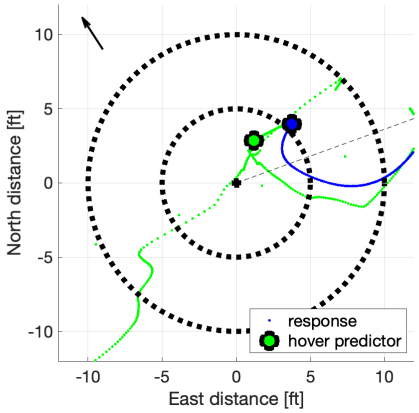

Fig. 28 Ground track around the helipad for AHA-1

1. Deceleration characteristics

Fig. 29 shows the deceleration profile during this maneuver in a similar fashion as was done for AHA-0 in Fig. 20 and AHA-1 in Fig. 25. The pressing of the hover button (to engage hover point transition) is marked by the red vertical dashed line in the thrust stick activity plot around 0.3 nm along track distance. Fig. 29(a) shows how the automatic deceleration is activated by engaging the hover point transition in AHA-2. From that moment onward, the vehicle decelerates automatically around 4 ft/s^2 (equals 2.5 kts/s) as dictated by $\dot{V}_{\text{hover}}$ (explained in detail in Sec. III.A.4) without pulling back the thrust stick manually. The thrust stick can be used to override the automatic deceleration rate. In contrast to the AHA-1 concept discussed in Sec. IV.D.2, no further thrust stick adjustments are needed in the hover engaged phase since the vehicle proceeds to the hover target which is latched to the center point in the landing zone, as can be seen by comparing Fig. 29(b) and Fig. 25(b). Comparing both these figures also shows a noticeable increase in comfort for AHA-2 due to the lack of sudden changes in accelerations/decelerations and ground speed, thanks to the absence of further thrust stick inputs. This difference also improves battery energy consumption in this phase.

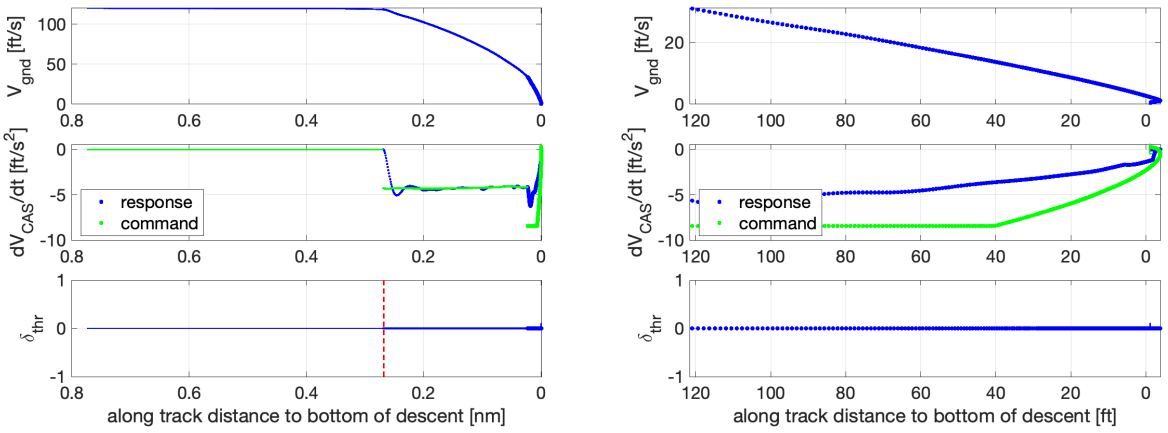

(a) Full run (b) Final phase

Fig. 29 Deceleration characteristics for AHA-2

2. Hover characteristics

Fig. 30 shows ground track in Fig. 30(a) and stick activity in Fig. 30(b) for the entire hover engaged phase. The ground track shows the actual position of the vehicle as well as the location of the stationary commanded hover location

(its marker in the figure is covered by the touchdown location marker due to the high precision of the hover target tracking controls). As it effectively is a hover target, it doesn't move during the transition maneuver, but it can be displaced by the pilot by moving the inceptors if necessary. In the course of the hover point engaged phase, the vehicle slowly converges to the hover target at constant altitude and with constant heading angle aligned with the reference path, and also compensates for a small downwind drift of less than 20 ft that accumulated during the hover transition phase. All this requires no pilot compensation at all as illustrated in Fig. 30(b). This is in sharp contrast to the three axes control task in hover for AHA-0 that was shown in Fig. 22(b) and the two axes control task for AHA-1 that was shown in Fig. 27(b). Very small longitudinal stick activity follows only at the very end, for touching down on the helipad, which was similar for both AHA-0 in Sec. IV.C.4 and AHA-1 in Sec. IV.D.4.

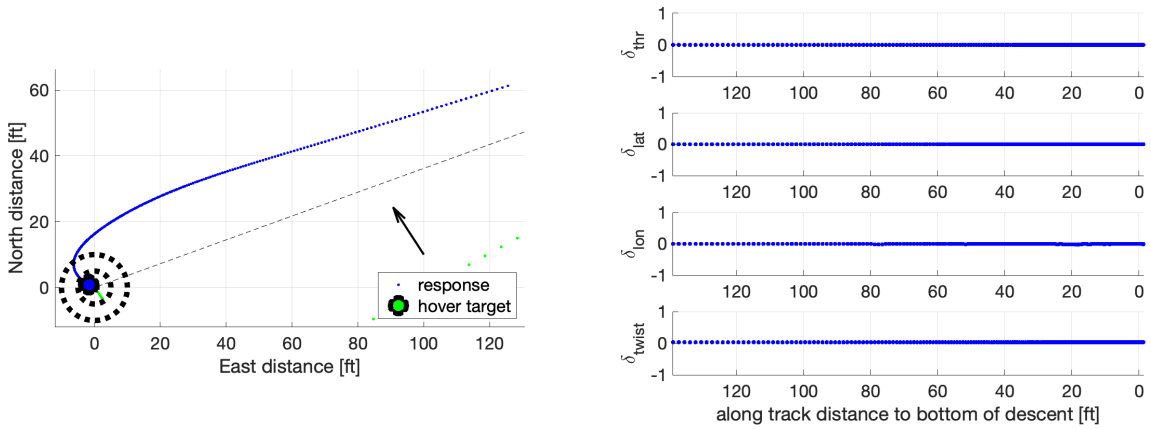

(a) Ground track

(b) Stick activity

Fig. 30 Hover characteristics for AHA-2

Fig. 31 zooms in on the ground track around the helipad, shows again both actual ground track and stationary commanded hover location (its marker in the figure is again covered by the touchdown location marker, even at this scale), and illustrates the ease to pinpoint the vehicle closer to the center of the circles, even in crosswind conditions. Also, the ground track is much smoother and the vehicle touches down closest to the helipad center location as compared to the performance of AHA-0 in Fig. 23 and of AHA-1 in Fig. 28.

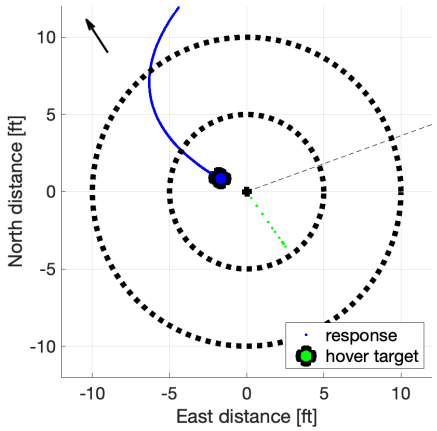

Fig. 31 Ground track around the helipad for AHA-2

V. Summary and Future Work

This paper focused on the development of a simplified vehicle control concept specifically designed for a lift-plus-cruise eVTOL vehicle with collective blade pitch lifting rotor controls. In standard operations, the SVC inceptors command acceleration and climb/descent rates combining the underlying heave, pitch and thrust axes of control to produce a consistent vehicle response across flight regimes. In addition, three hover automation conditions were implemented, meant to provide the pilot with varying levels of assistance in conducting a hover landing. In the first condition, AHA-0, no augmentations are made in transitioning to hover. If hover is armed, once under 10kts, a hover mode is engaged where the inceptors command lateral and longitudinal ground referenced velocities (similar to TRC). The second condition, AHA-1, implemented a transition to hover which automatically initiated a nominal deceleration and an automatic decrab maneuver. The transition also switches the lateral command response to a vector-based track command. Further, with the predicted hover point display symbology added to the map display, this condition provides the pilot with cueing to help in determining when to begin the deceleration maneuver. The third condition, AHA-2, also includes these aforementioned features and display cues but moves to a higher augmentation mode. In AHA-2, the inceptors command a target hover position and includes a feature to initially latch to the helipad if the hover button is pressed with the predicted hover position sufficiently close to the landing site. In addition, an envelope protection system ensures that the given commands keep the aircraft within safe operating limits and some of them are also included on the Primary Flight Display to provide additional awareness of when the aircraft is approaching saturation margins.

Results illustrated that in a high-fidelity fixed-base simulator environment, the higher assisted hover automation conditions (AHA-1 and AHA-2) helped a research pilot complete an approach and landing task in high crosswind. The task clearly shows how the assisted hover modes reduce the (coordinated multi-axis) inputs required by the pilot. In AHA-0, high crosswinds result in large cross-track deviations, requiring significant pilot compensation across three axes (forward, lateral and directional) in addition to managing the altitude. In comparison, AHA-2 only required the pilot to manage the vertical axis. These improvements have the potential to not only reduce workload in the handling task, but also improve ride quality and battery energy consumption.

A follow-on piloted simulation evaluation will be performed in the Vertical Motion Simulator at NASA Ames Research Center. The study is designed to look at the workload and handling across the assisted hover conditions in more operationally representative, nominal but stressing approach to landing scenarios. The evaluation will include multiple pilots of varying backgrounds flying a full approach procedure. The independent variables will also include both a nominal (6-deg) and steep (12-deg) approach angles, varying wind directions and magnitudes with gusts, as well as the presence of external traffic. The study will investigate challenges associated with transitioning from forward flight to a vertical landing. It aims to assess whether the automation augmentation and added displays can assist pilots in predictably and repeatably landing with the required accuracy while achieving acceptable workload, ride comfort and battery usage.

Acknowledgments

The authors wish to thank the Airspace Operations and Safety Program's (AOSP) Air Mobility Pathfinder (AMP) project. The authors would like to acknowledge John Archdeacon, Loran Haworth, Nelson Iwai, Mietek Steglinski and Amber Villa.

VI. Appendices

A. Command Response Types

Command response types describe the overall system response to pilot inputs. In general, the command response types introduced below fall under two main categories:

- <State> Command - where a constant inceptor deflection produces a constant commanded state. Releasing the inceptor back to the neutral position results in a zero (or nominal) commanded state (e.g., wings level). Subsequently, this command is usually fed through a first-order lag filter with a time constant that serves as a reference model.
- <State 1> Command / <State 2> Hold - where a constant inceptor deflection produces a constant command for the first state. Releasing the inceptor back to the neutral position results in the second state being maintained, even in the presence of disturbances. This is accomplished by maintaining a commanded target. For example, Fig. 32 shows the block diagram of the target rate command target hold function. A constant inceptor deflection produces a constant target rate command, which is saturated by light envelope limits and protected against windup. Next this commanded rate is integrated towards a commanded target state. This target state command is again constrained between saturation limits that are based on flight envelope limits. Next, this target command is fed through a first-order lag filter with a time constant that serves as a reference model. For the ultimate commanded target that is fed to the outer loop controller, a feedforward term is added consisting of the saturated target rate command scaled by a time constant. This feedforward signal removes much of the time delay in the vehicle response.

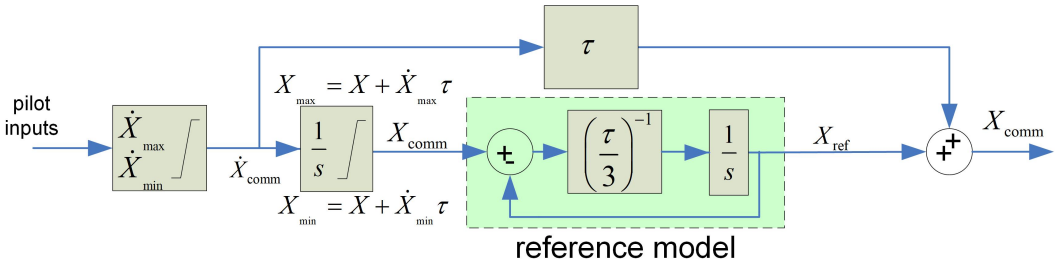

Fig. 32 Block diagram of the target rate command target hold function

1. Acceleration Command

For Acceleration Command (Accel-C), constant inceptor deflection results in a constant commanded acceleration. Releasing the inceptor back to the neutral position results in a zero acceleration command to maintain the current speed. The acceleration command is envelope protected (VI.B.1) and then sent to the Acceleration Control outer loop control system (VI.E.1).

2. Acceleration Command / Longitudinal Position Hold

For Acceleration Command / Longitudinal Position Hold (Accel-C/LonPos-H), a constant inceptor deflection result in a rate of change in the commanded target position along the longitudinal axis that is dependent upon the current groundspeed. Releasing the inceptor back to the neutral position will maintain the current commanded target position along the longitudinal axis. The acceleration command is envelope protected (VI.B.1), before being used to update the commanded target position in order to compute the corresponding acceleration command that is sent to the Acceleration Control outer loop control system (VI.E.1).

First the distance R from the target position is computed:

$$R = \sqrt{\Delta N^2 + \Delta E^2} \tag{23}$$

where N and E are the distances along North and East axes respectively:

$$\Delta N = (\text{lat}_{\text{cmd}} - \text{lat}) \cdot \frac{\pi}{180} \cdot R_e \tag{24}$$

$$\Delta E = (\text{lon}_{\text{cmd}} - \text{lon}) \cdot \frac{\pi}{180} \cdot R_e \cos \text{lat} \tag{25}$$

The target position is updated via the respective distance and speed changes based on the AHA hover deceleration rate $\dot{V}_{\text{hover}}$, first the deceleration is updated:

$$\Delta\dot{V}_{\text{cmd}} = \dot{V}_{\text{cmd}} - \dot{V}_{\text{hover}} \tag{26}$$

which is integrated for the change in commanded forward speed:

$$\Delta V_{X_{\text{cmd}}} = \Delta\dot{V}_{\text{cmd}} \cdot \Delta t \tag{27}$$

and is subsequently used for updating the change in forward distance:

$$\Delta X = \frac{1}{2}\frac{\Delta V_{X_{\text{cmd}}}^2 + 2\Delta V_{X_{\text{cmd}}} \cdot V_{\text{gnd}}}{\|\dot{V}_{\text{hover}}\|} \tag{28}$$

Finally the target position is updated by transforming the forward distance change in a lon and lat coordinates change:

$$\Delta\text{lat}_{\text{cmd}} = \Delta X \cdot \frac{\cos\psi}{R_e}\frac{180}{\pi} \tag{29}$$

$$\Delta\text{lon}_{\text{cmd}} = \Delta X \cdot \frac{\sin\psi}{R_e \cos\text{lat}}\frac{180}{\pi} \tag{30}$$

The last step is updating the acceleration command accordingly:

$$\dot{V}_{\text{cmd}} = -\frac{1}{2}\frac{V_{\text{gnd}}^2}{R} + \Delta\dot{V}_{\text{cmd}} \tag{31}$$

where distance R is provided by Eq. (23) and updated deceleration $\Delta\dot{V}_{\text{cmd}}$ by Eq. (26).

3. Bank Command

For Bank Command (Bank-C), a constant inceptor deflection results in a constant commanded bank angle. Releasing the inceptor back to the neutral position results in a zero commanded bank angle. The bank angle command is envelope protected (VI.B.2) and fed through a first-order lag filter with a time constant that serves as a reference model, and then sent to the Bank Control outer loop control system (VI.E.2).

4. Crab Command

For Crab Command Crab-C), a constant inceptor deflection results in a constant commanded crab angle. Releasing the inceptor back to the neutral position results in a zero commanded crab angle. The crab angle command is converted to a sideslip command (see Eq. (32)–(33)). This is achieved by first calculating the commanded sideslip rate $\dot{\beta}_{\text{cmd}}$:

$$\dot{\beta}_{\text{cmd}} = -\frac{1}{3\tau_\psi}\left(\psi_{\text{crab}_{\text{cmd}}} - \psi_{\text{crab}}\right) \tag{32}$$

where the crab angle ψ_{crab} is defined as the angle between vehicle forward X-axis and the ground speed velocity vector, and calculated as the difference between heading and track angle: $\psi_{\text{crab}} = \psi - \chi$. This commanded sideslip rate $\dot{\beta}_{\text{cmd}}$ is then used to incrementally update the commanded sideslip angle β_{cmd}:

$$\Delta\beta_{\text{cmd}} = \dot{\beta}_{\text{cmd}} \cdot \Delta t \tag{33}$$

which is envelope protected (VI.B.10) and sent to the Sideslip Control outer loop control system (VI.E.9).

5. Flight Path Angle Rate Command

For Flight Path Angle Rate Command (FPA-RC), a constant inceptor deflection results in a constant commanded flight path angle rate. Releasing the inceptor back to the neutral position results in a zero flight path angle rate command to maintain the current flight path angle. The flight path angle rate command is envelope protected (VI.B.4) and then sent to the FPA Rate Control outer loop control system (VI.E.4).

6. Flight Path Angle Rate Command / Flight Path Angle Hold

For Flight Path Angle Rate Command / Flight Path Angle Hold (FPA-RC/H), a constant inceptor deflection results in an envelope protected (VI.B.4) constant rate of change in the commanded flight path angle target. Releasing the inceptor back to the neutral position maintains the current commanded flight path angle target. A feedforward term, consisting of the flight path angle rate command scaled by a time constant, is added to the flight path angle target to generate the flight path angle command. This feedforward signal removes much of the time delay in the vehicle response. The resulting flight path angle command is sent to the Flight Path Angle Control outer loop control system (VI.E.3).

7. Heading Rate Command

For Heading Rate Command (Hdg-RC), a constant inceptor deflection results in a constant commanded heading rate. Releasing the inceptor back to the neutral position results in a zero heading rate command to maintain the current heading angle. The heading rate command is envelope protected (VI.B.5) and then sent to the Heading Rate Control outer loop control system (VI.E.5).

8. Lateral Acceleration Command / Track Hold

For Lateral Acceleration Command / Track Hold (LatAccel-C/Trk-H), a constant inceptor deflection results in an envelop protected (VI.B.6) constant rate of change in the commanded lateral velocity target. Releasing the inceptor back to a neutral position maintains the current track angle. This is achieved by augmenting the commanded lateral velocity target with a correction term so that track angle remains steady during acceleration or deceleration. The underlying concept is as follows. The track angle χ is defined as follows:

$$\chi = \arctan \frac{V_{\text{gnd}_{\text{East}}}}{V_{\text{gnd}_{\text{North}}}} \tag{34}$$

where $V_{\text{gnd}_{\text{East}}}$ is the East component of the earth referenced ground velocity vector and $V_{\text{gnd}_{\text{North}}}$ is the North component. The time derivative of the track angle is then derived as follows by means of the chain rule:

$$\dot{\chi} = \frac{1}{1 + \left(\frac{V_{\text{gnd}_{\text{East}}}}{V_{\text{gnd}_{\text{North}}}}\right)^2} \frac{d}{dt}\left(\frac{V_{\text{gnd}_{\text{East}}}}{V_{\text{gnd}_{\text{North}}}}\right) = \frac{\dot{V}_{\text{gnd}_{\text{East}}} V_{\text{gnd}_{\text{North}}} - \dot{V}_{\text{gnd}_{\text{North}}} V_{\text{gnd}_{\text{East}}}}{V^2_{\text{gnd}_{\text{North}}} + V^2_{\text{gnd}_{\text{East}}}} \tag{35}$$

For a steady track angle, one needs $\dot{\chi} = 0$, which results in the requirement that $\dot{V}_{\text{gnd}_{\text{East}}} V_{\text{gnd}_{\text{North}}} - \dot{V}_{\text{gnd}_{\text{North}}} V_{\text{gnd}_{\text{East}}} = 0$ for a nonzero denominator. This results in the following correction term for the lateral acceleration (after rotating all velocity components over ψ from North-East reference frame to body fixed reference frame):

$$\dot{V}_{\text{gnd}_{\text{Y}}} = \frac{V_{\text{gnd}_{\text{Y}}}}{V_{\text{gnd}_{\text{X}}}} \dot{V}_{\text{gnd}_{\text{X}}} \tag{36}$$

Thus, an additional track angle acceleration or deceleration term is needed before the usual rate-to-angle integrator:

- forward groundspeed $V_{\text{gnd}_{\text{X}}} > 0$:

$$\Delta\dot{V}_{Y_{\text{cmd}}} = \frac{V_{Y_{\text{cmd}}} \cdot \dot{V}_{\text{gnd}_{\text{X}}}}{\underline{V_{\text{gnd}_{\text{X}}}}} \tag{37}$$

- backward groundspeed $V_{\text{gnd}_{\text{X}}} < 0$:

$$\Delta\dot{V}_{Y_{\text{cmd}}} = \frac{V_{Y_{\text{cmd}}} \cdot \dot{V}_{\text{gnd}_{\text{X}}}}{\overline{V_{\text{gnd}_{\text{X}}}}} \tag{38}$$

Please note that both $V_{\text{gnd}_{\text{X}}}$ and $\dot{V}_{\text{gnd}_{\text{X}}}$ are defined in the body fixed reference frame (along the nose of the vehicle). The singularity protected denominators in Eq. (37) and (38) are defined as follows:

$$\underline{V_{\text{gnd}_{\text{X}}}} = \max\left(V_{\text{gnd}_{\text{X}}}, 20kts\right) \tag{39}$$

$$\overline{V_{\text{gnd}_{\text{X}}}} = \min\left(V_{\text{gnd}_{\text{X}}}, -20kts\right) \tag{40}$$

The resulting commanded lateral velocity target is sent to the lateral component of the Translational Rate Control outer loop control system (VI.E.12).

9. Lateral Velocity Command

For Lateral Velocity Command (LatVel-C), a constant inceptor deflection results in a constant commanded ground relative lateral velocity. Releasing the inceptor back to the neutral position results in a zero lateral velocity command to maintain the current lateral position. The lateral velocity command is envelope protected (VI.B.7) and then fed through a first-order lag filter with a time constant that serves as a reference model. The command is then sent to the lateral component of the Translational Rate Control outer loop control system (VI.E.12).

10. Longitudinal Velocity Command

For Longitudinal Velocity Command (LonVel-C), a constant inceptor deflection results in a constant commanded ground relative longitudinal velocity. Releasing the inceptor back to the neutral position results in a zero longitudinal velocity command to maintain the current longitudinal position. The longitudinal velocity command is envelope protected (VI.B.8) and then fed through a first-order lag filter with a time constant that serves as a reference model. The command is then sent to the longitudinal component of the Translational Rate Control outer loop control system (VI.E.12).

11. Position Rate Command / Position Hold

The Position Rate Command / Position Hold (Pos-RC/H) response type is separated into a lateral component (i.e., Lateral Velocity Command / Lateral Position Hold, or LatPos-RC/H) and a longitudinal component (i.e., Longitudinal Velocity Command / Longitudinal Position Hold, or LonPos-RC/H). Constant inceptor deflections result in envelope protected (VI.B.7 and VI.B.8) constant rates of change in the commanded target position along the respective (lateral and longitudinal) axes. Releasing the inceptors back to the neutral positions will maintain the current commanded target position. Subsequently, the command is protected against windup. Next this commanded rate is integrated towards a commanded position and converted to lat/lon coordinates as follows:

$$\Delta\text{lat}_\text{X} = V_{X_\text{cmd}} dt \cdot \frac{\cos\psi}{R_e} \cdot \frac{180}{\pi} \tag{41}$$

$$\Delta\text{lon}_\text{X} = V_{X_\text{cmd}} dt \cdot \frac{\sin\psi}{R_e \cos\text{lat}} \cdot \frac{180}{\pi} \tag{42}$$

$$\Delta\text{lat}_\text{Y} = V_{Y_\text{cmd}} dt \cdot \frac{-\sin\psi}{R_e} \cdot \frac{180}{\pi} \tag{43}$$

$$\Delta\text{lon}_\text{Y} = V_{Y_\text{cmd}} dt \cdot \frac{\cos\psi}{R_e \cos\text{lat}} \cdot \frac{180}{\pi} \tag{44}$$

Next the position command distances are computed (with $\text{lat}_\text{cmd} = \sum \Delta\text{lat}_\text{X} + \sum \Delta\text{lat}_\text{Y}$ and $\text{lon}_\text{cmd} = \sum \Delta\text{lon}_\text{X} + \sum \Delta\text{lon}_\text{Y}$):

$$\Delta N = (\text{lat}_\text{cmd} - \text{lat}) \cdot \frac{\pi}{180} \cdot R_e \tag{45}$$

$$\Delta E = (\text{lon}_\text{cmd} - \text{lon}) \cdot \frac{\pi}{180} \cdot R_e \cos\text{lat} \tag{46}$$

$$\Delta X = \Delta N \cos\psi + \Delta E \sin\psi \tag{47}$$

$$\Delta Y = \Delta E \cos\psi - \Delta N \sin\psi \tag{48}$$

The next step is to limit the position command distances for ΔX and ΔY in Eq. (47)–(48) between the limits $20kts \cdot \tau_\text{pos}$ and $-20kts \cdot \tau_\text{pos}$, where $\tau_\text{pos} = 3 \cdot \max\left(\tau_\phi, \tau_\theta\right)$. Finally the limited position command is computed with the reverse eq. (45) – (48). The speed control targets are calculated as follows:

$$V_{X_\text{cmd}} = \frac{1}{\tau_\text{pos}} \Delta X \tag{49}$$

$$V_{Y_\text{cmd}} = \frac{1}{\tau_\text{pos}} \Delta Y \tag{50}$$

The resulting commanded lateral and longitudinal velocities are sent to the Translational Rate Control outer loop control system (VI.E.12).

12. Roll Rate Command

For Roll Rate Command (Roll-RC), a constant inceptor deflection results in a constant commanded roll rate. Releasing the inceptor back to the neutral position results in a zero roll rate command to maintain the current bank angle. The roll rate command is envelope protected (VI.B.9) and then sent to the Roll Rate Control outer loop control system (VI.E.8).

13. Sideslip Command

For Sideslip Command (Slip-C), a constant inceptor deflection results in a constant commanded sideslip angle. Releasing the inceptor back to the neutral position results in a zero commanded sideslip angle. The sideslip angle command is envelope protected (VI.B.10) and fed through a first-order lag filter with a time constant that serves as a reference model, and then sent to the Sideslip Control outer loop control system (VI.E.9).

14. Track Rate Command / Lateral Position Hold

For Track Angle Rate Command / Lateral Position Hold (Trk-RC/LatPos-H), a constant inceptor deflection results in an envelope protected (VI.B.5) variable rate of change in the commanded target position along the lateral axis. Releasing the inceptor back to the neutral position will maintain the current commanded target position along the lateral axis. Subsequently, the command is protected against windup. The resulting track angle command is sent to the Track Angle Control outer loop control system (VI.E.10).

The position command is updated via the commanded track rate as follows:

$$\Delta\text{lat} = V_{Y_{\text{cmd}}} \cdot \Delta t \cdot \frac{-\sin\psi}{R_e} \frac{180}{\pi} \tag{51}$$

$$\Delta\text{lon} = V_{Y_{\text{cmd}}} \cdot \Delta t \cdot \frac{\cos\psi}{R_e \cos\text{lat}} \frac{180}{\pi} \tag{52}$$

with the commanded lateral speed component dependent on the commanded track rate as follows:

$$V_{Y_{\text{cmd}}} = R \cos\psi_{\text{crab}} \dot{\chi}_{\text{cmd}} \tag{53}$$

with distance R provided by Eq. (23) and crab angle $\psi_{\text{crab}} = \psi - \chi$ and track rate command $\dot{\chi}_{\text{cmd}}$ coming from the pilot.

The lateral position command distance ΔY follows from Eq. (48) and is used as a Y-position command. Combined with the longitudinal position command distance ΔX from Eq. (47), both are rewritten via

$$\Delta N = \Delta X \cos\psi - \Delta Y \sin\psi \tag{54}$$

$$\Delta E = \Delta X \sin\psi + \Delta Y \cos\psi \tag{55}$$

which are then used for the updating the commanded lat and lon coordinates:

$$\text{lat}_{\text{cmd}} = \text{lat} + \frac{\Delta N}{R_e} \frac{180}{\pi} \tag{56}$$

$$\text{lon}_{\text{cmd}} = \text{lon} + \frac{\Delta E}{R_e \cos\text{lat}} \frac{180}{\pi} \tag{57}$$

Subsequently, the same N and E components from (54) and (55) are used for calculating the track command:

$$\chi_{\text{cmd}} = \arctan\frac{E}{N} \tag{58}$$

and this angle is subsequently limited between $-\pi$ and π and followed by a back course correction:

$$\Delta\chi = \chi_{\text{cmd}} - \chi \tag{59}$$

where both measured track χ as well as the back course correction $\Delta\chi$ are limited between $-\pi$ and π, and finalized by the following corrections:

- if $\Delta\chi > \frac{\pi}{2}$:

$$\Delta\chi = \pi - \Delta\chi \tag{60}$$

$$\chi_{\text{cmd}} = \Delta\chi + \chi \tag{61}$$

- elseif $\Delta\chi < -\frac{\pi}{2}$:

$$\Delta\chi = -\pi - \Delta\chi \tag{62}$$
$$\chi_{\text{cmd}} = \Delta\chi + \chi \tag{63}$$

15. Track Rate Command / Track Hold

For Track Target Rate Command / Track Target Hold (Trk-RC/H), a constant inceptor deflection results in an envelope protected (VI.B.5) constant rate of change in the commanded track angle target. Releasing the inceptor back to the neutral position maintains the current commanded track angle target. A feedforward term, consisting of the track rate command scaled by a time constant, is added to the track angle target to generate the track angle command. This feedforward signal removes much of the time delay in the vehicle response. The maximum change in the resulting track angle command $\Delta\chi$ is limited based on the maximum turn rate as follows:

$$\chi_{\text{cmd}} = \chi + \Delta\chi_{\text{cmd}} \tag{64}$$

where the commanded change in track angle $\Delta\chi_{\text{cmd}}$ is restricted between the two limits:

$$\Delta\chi_{\max} = \min\left(\dot{\psi}_{\max} \cdot \tau_{\chi}, 45deg\right) \tag{65}$$
$$\Delta\chi_{\min} = \max\left(\dot{\psi}_{\min} \cdot \tau_{\chi}, -45deg\right) \tag{66}$$

The resulting track angle command is sent to the Track Control outer loop control system (VI.E.10).

16. Vertical Acceleration Command / Flight Path Angle Hold

For Vertical Acceleration Command / Flight Path Angle Hold (VertAccel-C/FPA-H), a constant inceptor deflection results in an envelope protected (VI.B.11) constant vertical acceleration command, which gets integrated into a commanded vertical speed target. Releasing the inceptor back to a neutral position maintains the current flight path angle. This is achieved by augmenting the commanded vertical velocity target with a correction term so that flight path angle remains steady during acceleration or deceleration. The underlying concept is as follows. The flight path angle γ is defined as follows:

$$\gamma = \arctan\frac{V_{\text{gnd}_Z}}{V_{\text{gnd}_X}} \tag{67}$$

where V_{gnd_Z} is the vertical component of the earth referenced velocity vector and V_{gnd_X} is the forward component along the flight path. The time derivative of the flight path angle is then derived as follows by means of the chain rule:

$$\dot{\gamma} = \frac{1}{1 + \left(\frac{V_{\text{gnd}_Z}}{V_{\text{gnd}_X}}\right)^2}\frac{d}{dt}\left(\frac{V_{\text{gnd}_Z}}{V_{\text{gnd}_X}}\right) = \frac{\dot{V}_{\text{gnd}_Z}V_{\text{gnd}_X} - \dot{V}_{\text{gnd}_X}V_{\text{gnd}_Z}}{V_{\text{gnd}_X}^2 + V_{\text{gnd}_Z}^2} \tag{68}$$

For a steady flight path angle, one needs $\dot{\gamma} = 0$, which results in the requirement that $\dot{V}_{\text{gnd}_Z}V_{\text{gnd}_X} - \dot{V}_{\text{gnd}_X}V_{\text{gnd}_Z} = 0$ for a nonzero denominator. This results in the following correction term for the vertical acceleration:

$$\dot{V}_{\text{gnd}_Z} = \frac{V_{\text{gnd}_Z}}{V_{\text{gnd}_X}}\dot{V}_{\text{gnd}_X} \tag{69}$$

Thus, an additional flight path angle acceleration or deceleration term is needed before the usual rate-to-angle integrator, as follows:

- forward groundspeed $V_{\text{gnd}_X} > 0$:

$$\Delta\dot{V}_{Z_{\text{cmd}}} = \frac{V_{Z_{\text{cmd}}} \cdot \dot{V}_{\text{gnd}_X}}{V_{\text{gnd}_X}} \tag{70}$$

- backward groundspeed $V_{\text{gnd}_X} < 0$:

$$\Delta\dot{V}_{Z_{\text{cmd}}} = \frac{V_{Z_{\text{cmd}}} \cdot \dot{V}_{\text{gnd}_X}}{V_{\text{gnd}_X}} \tag{71}$$

Please note that both V_{gnd_X} and $\dot{V}_{\text{gnd}_X}$ are defined in the body fixed reference frame (along the nose of the vehicle). The singularity protected denominators in Eq. (70) and (71) are defined as follows:

$$\underline{V_{\text{gnd}_X}} = \max\left(V_{\text{gnd}_X}, 20kts\right) \tag{72}$$

$$\overline{V_{\text{gnd}_X}} = \min\left(V_{\text{gnd}_X}, -20kts\right) \tag{73}$$

This singularity protection also makes the commanded flight path level off when approaching hover. Moreover, the vertical acceleration limits are defined as follows: $\dot{V}_{Z_{\max}} = \frac{V_{Z_{\max}}}{\tau_\gamma}$ and $\dot{V}_{Z_{\min}} = \frac{V_{Z_{\min}}}{\tau_\gamma}$. The resulting commanded vertical speed target is sent to the Vertical Speed Control outer loop control system (VI.E.13).

17. Vertical Speed Command

For Vertical Speed Command (Vspd-C), a constant inceptor deflection results in a constant commanded vertical speed. Releasing the inceptor back to the neutral position results in a zero vertical speed command to maintain the current altitude. The vertical speed command is envelope protected (VI.B.12) and fed through a first-order lag filter with a time constant that serves as a reference model, and then sent to the Vertical Speed Control outer loop control system (VI.E.13).

B. Command Protection Envelope Limits

Envelope limits are computed for each type of command that is generated by the different command response types. Several additional estimated envelope limits are computed for display purposes, in order to enhance envelope awareness. These are discussed in Appendix VI.C.

1. Acceleration/Deceleration Limits

Acceleration/deceleration limits ($\dot{V}_{\max}$,$\dot{V}_{\min}$) are dependent upon the flight regime. During the forward flight and transitional regimes, the acceleration/deceleration limits are calculated such that the airspeed limits are not exceeded:

$$\dot{V}_{\max} = \min\left(\dot{V}_{\text{CAS}_{\max}}, \frac{1}{\tau_V}\left(V_{\text{CAS}_{\max}} - V_{\text{CAS}}\right)\right) \tag{74}$$

$$\dot{V}_{\min} = \max\left(\dot{V}_{\text{CAS}_{\min}}, \frac{1}{\tau_V}\left(V_{\text{CAS}_{\min}} - V_{\text{CAS}}\right)\right) \tag{75}$$

The limits for the CAS acceleration/deceleration $\dot{V}_{\text{CAS}_{\max}}$,$\dot{V}_{\text{CAS}_{\min}}$ are specified to ±10 knots/s.

2. Bank Limits

Bank angle limits ($\phi_{\max}$,$\phi_{\min}$) are dependent upon the flight regime. The bank angle limit ranges from ±45°in the forward flight regime, down to ±30°in the transitional regime. During the hover regime, the bank angle limits are calculated such that the lateral acceleration limits (VI.B.6) are not exceeded:

$$\phi_{\max} = \arcsin\left(\frac{\cos\phi}{g}\left(\dot{v}_{Y_{\max}} - \dot{v}_Y\right) + \sin\phi\right) \tag{76}$$

$$\phi_{\min} = \arcsin\left(\frac{\cos\phi}{g}\left(\dot{v}_{Y_{\min}} - \dot{v}_Y\right) + \sin\phi\right) \tag{77}$$

where the arcsin arguments $\left(\frac{\cos\phi}{g}\left(\dot{v}_{Y_{\max}} - \dot{v}_Y\right) + \sin\phi\right)$ and $\left(\frac{\cos\phi}{g}\left(\dot{v}_{Y_{\min}} - \dot{v}_Y\right) + \sin\phi\right)$ are limited between -1 and 1. Moreover $\phi_{\max}$ and $\phi_{\min}$ are fed through a first order lag filter to slow down their changes.

3. Flight Path Angle Limits

The envelope flight path angle limits depend on the flight condition and are only used above 34 kts groundspeed. In the hover regime they are calculated based on the vertical speed limits:

$$\gamma_{\max_{\text{env}}} = \arctan \frac{V_{Z_{\max}}}{V_{\text{gnd}}} \tag{78}$$

$$\gamma_{\min_{\text{env}}} = \arctan \frac{V_{Z_{\min}}}{V_{\text{gnd}}} \tag{79}$$

In transition and forward flight, the flight path angle limits are calculated such that speed limits are prioritized:

$$\gamma_{\max_{\text{env}}} = \min\left(\gamma_{\max_{\text{ctl}}}, \gamma_{V_{\text{CAS}}+5\text{kts}}\right) \tag{80}$$

$$\gamma_{\min_{\text{env}}} = \min\left(\gamma_{\min_{\text{ctl}}}, -\gamma_{V_{\text{CAS}}-5\text{kts}}\right) \tag{81}$$

after which $\gamma_{\max_{\text{env}}}$ and $\gamma_{\min_{\text{env}}}$ are fed through a first order lag filter to slow down their changes. In Eq. (80)–(81), the quantities $\gamma_{V_{\text{CAS}}}$ are flight path angles based on a certain calibrated target speed. They are calculated as follows:

$$\gamma_{V_{\text{CAS}}} = \arcsin\left(\sin\gamma - \frac{\dot{V}_{\text{TAS}_{\text{cmd}}} - \dot{V}_{\text{TAS}}}{g}\right) \tag{82}$$

where the arcsin argument $\left(\sin\gamma - \frac{\dot{V}_{\text{TAS}_{\text{cmd}}} - \dot{V}_{\text{TAS}}}{g}\right)$ is limited between -1 and 1. $\dot{V}_{\text{TAS}_{\text{cmd}}}$ consists of a limited term that is based on a limited speed error $\dot{V}_{\Delta V}$ and an additional term that compensates for thrust based speed acceleration or deceleration limits, and which differs for climb and descent:

$$\dot{V}_{\text{TAS}_{\text{cmd}}} = \dot{V}_{\Delta V} - X_{u_{\delta_{\text{thr}}}}(1 - \delta_{\text{thr}}) \quad \text{for climb} \tag{83}$$

$$\dot{V}_{\text{TAS}_{\text{cmd}}} = \dot{V}_{\Delta V} + X_{u_{\delta_{\text{thr}}}}\delta_{\text{thr}} \quad \text{for descent} \tag{84}$$

where $X_{u_{\delta_{\text{thr}}}}$ is the coefficient that calculates the impact of a throttle change on the forward speed component. Moreover, $\dot{V}_{\Delta V}$ is limited between the previously defined $\dot{V}_{\min_{\text{env}}}$ and $\dot{V}_{\max_{\text{env}}}$ (see Eq. (74)–(75)) and where:

$$\dot{V}_{\Delta V} = \frac{1}{\tau_V}\Delta_V + \varepsilon_{\text{corr}_{\text{IAS}\to\text{TAS}}} \tag{85}$$

where $\varepsilon_{\text{corr}_{\text{IAS}\to\text{TAS}}}$ is a correction term for the conversion from indicated airspeed (IAS, with which the target is defined) to true airspeed (TAS, with which the flight path angle is calculated). The limited speed error ΔV itself is calculated as follows:

$$\Delta V = V_{\text{TAS}_{\text{target}}} - V_{\text{TAS}} \tag{86}$$

which is also limited between $\dot{V}_{\text{CAS}_{\min}} \cdot \tau_V$ and $\dot{V}_{\text{CAS}_{\max}} \cdot \tau_V$.

4. Flight Path Angle Rate Limits

The envelope flight path angle rate limits ($\dot{\gamma}_{\max}$,$\dot{\gamma}_{\min}$) are calculated such that the flight path angle limits are not exceeded:

$$\dot{\gamma}_{\max} = \min\left(\dot{\gamma}_{\text{ctl}_{\max}}, \dot{\theta}_{\max}, \frac{1}{\tau_\gamma}(\gamma_{\max} - \gamma)\right) \tag{87}$$

$$\dot{\gamma}_{\min} = \max\left(\dot{\gamma}_{\text{ctl}_{\min}}, \dot{\theta}_{\min}, \frac{1}{\tau_\gamma}(\gamma_{\min} - \gamma)\right) \tag{88}$$

with the flight path angle limits $\gamma_{\max}$,$\gamma_{\min}$ defined in Sec. VI.B.3 and where:

$$\dot{\theta}_{\max} = \min\left(\dot{\theta}_{\text{ctl}_{\max}}, \frac{1}{\tau_\theta}(\theta_{\max} - \theta)\right) \tag{89}$$

$$\dot{\theta}_{\min} = \max\left(\dot{\theta}_{\text{ctl}_{\min}}, \frac{1}{\tau_\theta}(\theta_{\min} - \theta)\right) \tag{90}$$

with the control limits for the flight path angular rates specified as:

$$\dot{\gamma}_{\text{ctl}_{\max}} = \min\left(\dot{\theta}_{\text{ctl}_{\max}}, \frac{\gamma_{\text{ctl}_{\max}}}{\tau_\gamma}\right) \tag{91}$$

$$\dot{\gamma}_{\text{ctl}_{\min}} = \max\left(\dot{\theta}_{\text{ctl}_{\min}}, \frac{\gamma_{\text{ctl}_{\min}}}{\tau_\gamma}\right) \tag{92}$$

5. Heading Rate Limits

Heading (or turn) rate limits ($\dot{\psi}_{\max}$,$\dot{\psi}_{\min}$) are dependent upon the flight regime. During forward flight and transitional regimes, the heading rate limits are calculated such that the bank angle limits (VI.B.2) are not exceeded:

$$\dot{\psi}_{\max} = \frac{g \tan\phi_{\max}}{V_{\text{TAS}_{\text{lim}}} \cos\theta_{\text{lim}}} \tag{93}$$

$$\dot{\psi}_{\min} = \frac{g \tan\phi_{\min}}{V_{\text{TAS}_{\text{lim}}} \cos\theta_{\text{lim}}} \tag{94}$$

The Appendices in [11] derive Eq. (93),(94). These limits are first order filtered to slow down their changes.

During the hover regime, the heading rate limits are calculated such that the specified yaw rate limits (of ±22°/sec) are not exceeded:

$$\dot{\psi}_{\max} = \max\left(\frac{q_{\max}\sin\phi + r_{\max}\cos\phi}{\cos\theta_{\text{lim}}}, \frac{q_{\min}\sin\phi + r_{\min}\cos\phi}{\cos\theta_{\text{lim}}}\right) \tag{95}$$

$$\dot{\psi}_{\min} = \min\left(\frac{q_{\max}\sin\phi + r_{\max}\cos\phi}{\cos\theta_{\text{lim}}}, \frac{q_{\min}\sin\phi + r_{\min}\cos\phi}{\cos\theta_{\text{lim}}}\right) \tag{96}$$

The denominators $V_{\text{TAS}_{\text{lim}}}$ in Eq. (93),(94) and $\cos\theta_{\text{lim}}$ in Eq. (93)–(96) are singularity protected as follows:

$$V_{\text{TAS}_{\text{lim}}} = \max\left(V_{\text{TAS}}, 10 \text{ kts}\right) \tag{97}$$

$$\cos\theta_{\text{lim}} = \text{sgn}\left(\cos\theta\right) \max\left(|\cos\theta|, 0.005\right) \tag{98}$$

6. Lateral Acceleration Limits

Lateral acceleration limits () are only utilized during the hover regime. The limits for the lateral component of ground referenced acceleration are calculated such that the lateral velocity limits (VI.B.7) are not exceeded:

$$\dot{v}_{Y_{\max}} = \frac{1}{\tau_V}\left(v_{Y_{\max}} - v_{\text{gnd}}\right) \tag{99}$$

$$\dot{v}_{Y_{\min}} = \frac{1}{\tau_V}\left(v_{Y_{\min}} - v_{\text{gnd}}\right) \tag{100}$$

7. Lateral Velocity Limits

Lateral velocity limits ($v_{Y_{\max}}$,$v_{Y_{\min}}$) are only utilized during the hover regime. The limits for the lateral component of groundspeed are specified to ±20 knots.

8. Longitudinal Velocity Limits

Longitudinal velocity limits ($v_{X_{\max}}$,$v_{X_{\min}}$) are only utilized during the hover regime. The limits for the longitudinal component of groundspeed are specified to ±20 knots.

9. Roll Rate Limits

Roll rate limits ($p_{\max}$,$p_{\min}$) are based on bank angle limits (VI.B.2):

$$p_{\max} = \max\left(\dot{\phi}_{\max} - \dot{\psi}\sin\theta, \dot{\phi}_{\min} - \dot{\psi}\sin\theta\right) \tag{101}$$

$$p_{\min} = \min\left(\dot{\phi}_{\max} - \dot{\psi}\sin\theta, \dot{\phi}_{\min} - \dot{\psi}\sin\theta\right) \tag{102}$$

$$\text{with:} \quad \dot{\phi}_{\max} = \frac{1}{\tau_\phi}\left(\phi_{\max} - \phi\right) \quad \text{and} \quad \phi_{\min} = \frac{1}{\tau_\phi}\left(\phi_{\min} - \phi\right) \tag{103}$$

10. Sideslip Limits

Sideslip limits ($\beta_{\max}$,$\beta_{\min}$) are only utilized during the forward flight and transitional regimes. The limits for sideslip are specified to ±15°.

11. Vertical Acceleration Limits

These envelope protections work as follows:

$$\dot{V}_{Z_{\max}} = \frac{V_{Z_{\max}}}{\tau_\gamma} \tag{104}$$

$$\dot{V}_{Z_{\min}} = \frac{V_{Z_{\min}}}{\tau_\gamma} \tag{105}$$

where the vertical velocity limits $V_{Z_{\max}}$,$V_{Z_{\min}}$ are specified in Sec. VI.B.12.

12. Vertical Velocity Limits

The vertical velocity limits depend on the flight regime. In the hover regime, they are defined by their respective control limits which are specified as ±3,000 ft per minute. In transition and forward flight, they are based on the maximum flight path angle or the maximum pitch attitude angle, whichever one is the strictest:

$$V_{Z_{\max}} = \tan\left(\min\left(\gamma_{\max}, \theta_{\max} - \alpha\right)\right) \cdot V_{\text{gnd}} \tag{106}$$

$$V_{Z_{\min}} = \tan\left(\max\left(\gamma_{\min}, \theta_{\min} - \alpha\right)\right) \cdot V_{\text{gnd}} \tag{107}$$

where the flight path angle limits are specified in Sec. VI.B.3 and the pitch attitude angle limits are specified in

C. Awareness Envelope Limits

The following awareness envelope limits are shown on the PFD:

1) min and max CAS: $V_{\text{CAS}_{\min}}$ and $V_{\text{CAS}_{\max}}$ are estimated based on margins to saturation limits of the throttle inputs.
2) min and max vertical speed: $\dot{h}_{\min}$ and $\dot{h}_{\max}$ are estimated based on margins to saturation limits of the equivalent collective inputs.
3) min and max bank angle: $\phi_{\min}$ and $\phi_{\max}$
4) min and max sideslip angle: $\beta_{\min}$ and $\beta_{\max}$

The awareness limits for bank angle and sideslip as shown on the PFD are independent of the margins to input saturation and are identical to the command protection envelope limits as discussed in Sec. VI.B.2 and VI.B.10 respectively.

1. Calibrated Airspeed CAS

The envelope limits for CAS are based on the margins until saturation of the throttle inputs, which impact the maximum acceleration/deceleration capability as follows:

$$\dot{V}_{\text{CAS}_{\max}} = \dot{V}_{\text{CAS}} + \dot{u}_{\delta_{\text{thr}}}(1 - \delta_{\text{thr}_{\text{comm}}}) \tag{108}$$

$$\dot{V}_{\text{CAS}_{\min}} = \dot{V}_{\text{CAS}} + \dot{u}_{\delta_{\text{thr}}}(0 - \delta_{\text{thr}_{\text{comm}}}) \tag{109}$$

where $\dot{u}_{\delta_{\text{thr}}}$ is a control derivative that quantifies the contribution of the throtle to the forward acceleration in body axis. These limits can then be used to calculate the maximum and minimum speed:

$$V_{\text{CAS}_{\max}} = V_{\text{CAS}} + \dot{V}_{\text{CAS}_{\max}} \cdot 3\tau_V \tag{110}$$

$$V_{\text{CAS}_{\min}} = V_{\text{CAS}} + \dot{V}_{\text{CAS}_{\min}} \cdot 3\tau_V \tag{111}$$

where τ_V is the time constant for the airspeed V.

2. Vertical Speed $\dot{h}$

The envelope limits for the vertical speed are based on the margins until saturation of the equivalent collective inputs, which impact the maximum vertical acceleration/deceleration capability in the following way:

$$\dot{V}_{Z_{\max}} = \dot{V}_Z + \cos\phi\cos\theta \cdot \dot{w}_{\delta_{\text{coll}}}(1 - \delta_{\text{coll}_{\text{comm}}}) \tag{112}$$

$$\dot{V}_{Z_{\min}} = \dot{V}_Z + \cos\phi\cos\theta \cdot \dot{w}_{\delta_{\text{coll}}}(-1 - \delta_{\text{coll}_{\text{comm}}}) \tag{113}$$

where $\dot{w}_{\delta_{\text{coll}}}$ is a control derivative that quantifies the contribution of the collective to the vertical acceleration in body axis. These limits can then be used to calculate the maximum climb and sink rate:

$$\dot{h}_{\max} = \dot{h} + \dot{V}_{Z_{\max}} \cdot 3\tau_\gamma \tag{114}$$

$$\dot{h}_{\min} = \dot{h} + \dot{V}_{Z_{\min}} \cdot 3\tau_\gamma \tag{115}$$

where τ_γ is the time constant for the flight path angle γ.

D. Automatic Trim

Automatic trim is used to enhance the acceleration and deceleration rate of the vehicle, by taking advantage of the additional axis of control. The automatic trim commands pitch in the hover regime, and angle of attack (i.e., using heave) in the transitional regime.

1. Angle of Attack Trim

For angle of attack trim, a commanded angle of attack α is calculated that corresponds to a given normalized thrust setting, according to the following mapping:

$$\alpha_{\text{cmd}} = (\alpha_{\min} - \alpha_{\max})\, \delta_{\text{thr}} + \alpha_{\max} \tag{116}$$

where $\alpha_{\min} = 0deg$ and $\alpha_{\max} = 10deg$ and δ_{thr} is the normalized thrust setting, between 0 and 1. Subsequently, this command is sent through a first order filter that serves as reference model:

$$\dot{\alpha}_{\text{ref}} = \frac{1}{\tau_\alpha} (\alpha_{\text{cmd}} - \alpha_{\text{ref}}) \tag{117}$$

The resulting angle of attack command is sent to the Angle of Attack Command (AOAC) inner loop control system (VI.F.2).

2. Pitch Trim

For pitch trim, a pitch attitude angle θ is calculated that corresponds to a given normalized thrust setting, according to the following mapping:

$$\theta_{\text{cmd}} = (\theta_{\min} - \theta_{\max})\, \delta_{\text{thr}} + \theta_{\max} \tag{118}$$

where $\theta_{\min} = 0deg$ and $\theta_{\max} = 10deg$ and δ_{thr} is the normalized thrust setting, between 0 and 1. Subsequently, this command is sent through a first order filter that serves as reference model:

$$\dot{\theta}_{\text{ref}} = \frac{1}{\tau_\theta} (\theta_{\text{cmd}} - \theta_{\text{ref}}) \tag{119}$$

The resulting pitch angle command is sent to the Pitch Angle Control outer loop control system (VI.E.6).

E. Outer Loop Control Systems

There outer loop control systems introduced in Fig. 10 are explained below. In general, they fall under four main categories:

- Euler and aerodynamic angles and rates
- Navigation angles and rates
- Altitude and vertical speed
- Speed and acceleration

1. Acceleration Control

For acceleration control, the commanded acceleration $\dot{V}_{\text{cmd}}$ is passed directly to the ACSH inner loop control system (VI.F.1), which controls the rate of change of airspeed in the forward flight and transitional regimes, and the rate of change of forward groundspeed in the hover regime.

2. Bank Control

For bank angle control, the commanded bank angle ϕ_{cmd} is used to calculate the controlled earth referenced bank rate command $\dot{\phi}_{\text{cmd}}$, based on the bank time constant τ_ϕ, as follows:

$$\dot{\phi}_{\text{cmd}} = \frac{1}{\tau_\phi}\left(\phi_{\text{cmd}} - \phi\right) \tag{120}$$

Subsequently, a coordinate transformation is performed, from earth referenced to body fixed:

$$p_{\text{cmd}} = \dot{\phi}_{\text{cmd}} - \dot{\psi}\sin\theta \tag{121}$$

This roll rate command is subsequently fed to the roll rate control outer loop control system (VI.E.8).

3. Flight Path Angle Control

For flight path angle control, the commanded flight path angle γ_{cmd} is used to control the flight path angle either by pitch via $\dot{\gamma}_{\text{cmd}}$ (in the forward flight and transitional regimes), or by heave via $\dot{h}_{\text{cmd}}$ (in the hover regime).

Flight Path Angle By Pitch:

For flight path angle by pitch, the flight path angle command is used to calculate the flight path angle rate command:

$$\dot{\gamma}_{\text{cmd}} = \frac{1}{\tau_\gamma}\left(\gamma_{\text{cmd}} - \gamma\right) \tag{122}$$

and is then sent to the flight path angle rate control outer loop control system (VI.E.4).

Flight Path Angle By Heave:

For flight path angle by heave, the commanded flight path angle is converted to a vertical speed command: ($\dot{h}_{\text{cmd}}$):

$$\dot{h}_{\text{cmd}} = \tan\gamma_{\text{cmd}} \cdot V_{\text{gnd}_{\text{lim}}} \tag{123}$$

where $V_{\text{gnd}_{\text{lim}}}$ is the lower value limited ground speed, defined as follows:

$$V_{\text{gnd}_{\text{lim}}} = \max\left(V_{\text{gnd}}, 20kts\right) \tag{124}$$

The commanded vertical speed is then sent to the vertical speed control outer loop control system (VI.E.13).

4. Flight Path Angle Rate Control

For flight path angle rate control, the commanded flight path angle rate $\dot{\gamma}_{\text{cmd}}$ is used to control the flight path angle rate either by pitch (in the forward flight and transitional regimes), or by heave via $\dot{h}_{\text{cmd}}$ (in the hover regime).

Flight Path Angle Rate By Pitch:

For flight path angle rate by pitch, the assumption is made that the commanded pitch rate can be approximated by the commanded flight path angle rate (i.e., $\dot{\theta}_{\text{cmd}} \approx \dot{\gamma}_{\text{cmd}}$). Subsequently, a coordinate transformation is performed, from earth referenced to body fixed:

$$q_{\text{cmd}} = \dot{\theta}_{\text{cmd}}\cos\phi + \dot{\psi}\cos\theta\sin\phi \tag{125}$$

This pitch rate command is subsequently fed to the pitch rate control outer loop control system (VI.E.7).

Flight Path Angle Rate By Heave:

For flight path angle rate by heave, the commanded flight path angle is calculated:

$$\gamma_{\text{cmd}} = \gamma + \tau_\gamma\dot{\gamma}_{\text{cmd}} \tag{126}$$

This commanded flight path angle is then used to calculate the commanded vertical speed:

$$\dot{h}_{\text{cmd}} = \tan\gamma_{\text{cmd}} \cdot V_{\text{gnd}} \tag{127}$$

where V_{gnd} is the ground speed. The commanded vertical speed is then sent to the vertical speed control outer loop control system (VI.E.13).

5. Heading Rate Control

Heading rate control is only utilized during the hover regime. The commanded heading rate $\dot{\psi}_{\text{cmd}}$ is passed directly to the RCDH inner loop control system (VI.F.4).

6. Pitch Angle Control

For pitch angle control, the commanded pitch attitude angle θ_{cmd} is used to calculate the controlled earth referenced pitch rate $\dot{\theta}_{\text{cmd}}$, based on the pitch time constant τ_θ, as follows:

$$\dot{\theta}_{\text{cmd}} = \frac{1}{\tau_\theta} \left(\theta_{\text{cmd}} - \theta\right) \tag{128}$$

Subsequently, a coordinate transformation is performed, from earth referenced to body fixed:

$$q_{\text{cmd}} = \dot{\theta}_{\text{cmd}} \cos\phi + \dot{\psi} \cos\theta \sin\phi \tag{129}$$

This pitch rate is then fed to the pitch rate control outer loop control system (VI.E.7).

7. Pitch Rate Control

For pitch rate control, the commanded pitch rate q_{cmd} is passed directly to the RCAH inner loop control system (VI.F.3).

8. Roll Rate Control

For roll rate control, the commanded roll rate p_{cmd} is passed directly to the RCAH inner loop control system (VI.F.3).

9. Sideslip Control

For sideslip control, the commanded sideslip angle β_{cmd} is passed directly to the turn coordination inner loop control system (VI.F.6).

10. Track Control

For track control, the commanded track angle χ_{cmd} is used to calculate the commanded track rate $\dot{\chi}_{\text{cmd}}$, based on the track time constant τ_χ, as follows:

$$\dot{\chi}_{\text{cmd}} = \frac{1}{\tau_\chi} \left(\chi_{\text{cmd}} - \chi\right) \tag{130}$$

This commanded track rate $\dot{\chi}_{\text{cmd}}$ is then fed to the track rate control outer loop control system (VI.E.11).

11. Track Rate Control

For track rate control, the commanded track rate $\dot{\chi}_{\text{cmd}}$ is used to control bank either for a turn (in the forward flight and transitional regimes) or for lateral translation (in the hover regime).

Track Rate By Turn:

For track rate by turn, one needs to calculate the commanded bank angle for controlling track rate but potentially in the presence of significant sideslip. The derivation follows next. The applicable Free Body Diagram of the governing forces is shown in Fig. 33.

The equation of motion along the body Y-axis Y_B is as follows:

$$W \sin\phi + Y_{\text{aero}} = mVr \tag{131}$$

where Y_{aero} is the aerodynamic sideforce, which is caused by the sideslipping flight. The inverse Euler equation for the body axis yaw rate r is defined as:

$$r = \dot{\psi} \cos\phi \cos\theta - \dot{\theta} \sin\phi \tag{132}$$

Combining Eq. (131) and (132) results in:

$$W \sin\phi + Y_{\text{aero}} = mV \left(\dot{\psi} \cos\phi \cos\theta - \dot{\theta} \sin\phi\right) \tag{133}$$

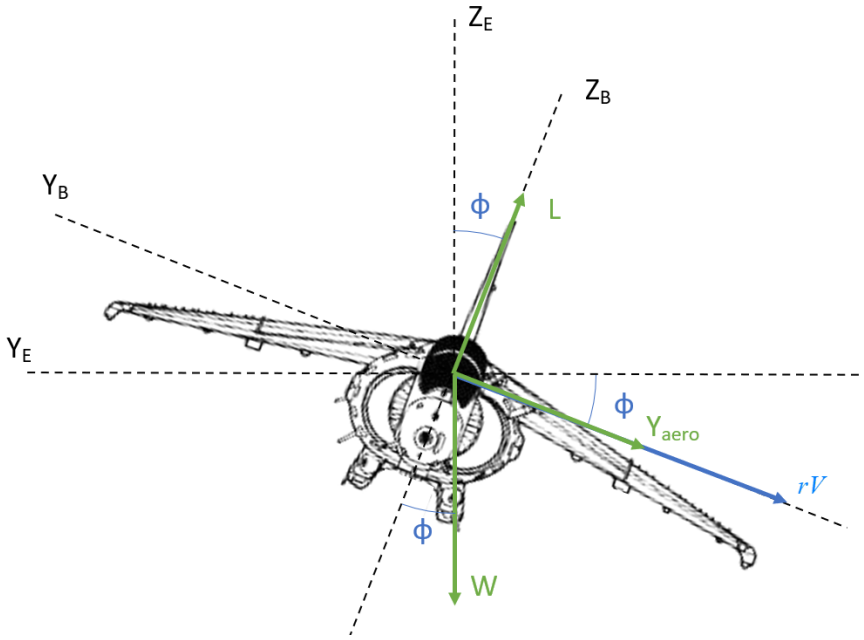

Fig. 33 Governing forces in turning flight along the Y_B and Z_B axes

Next substituting $W = mg$ and $Y_{\text{aero}} = n_Y W = n_Y mg$:

$$mg \sin\phi + n_Y mg = mV\left(\dot{\psi}\cos\phi\cos\theta - \dot{\theta}\sin\phi\right) \tag{134}$$

Eliminating the common mass factor m and regrouping for the ϕ terms:

$$\left(g + V\dot{\theta}\right)\sin\phi - \left(V\cos\theta\dot{\psi}\right)\cos\phi = -gn_Y \tag{135}$$

Solving for bank angle ϕ results in the equation, where the relevant required variables are used where necessary:

$$\phi_{\text{cmd}} = \arccos\left(\frac{-gn_Y}{\sqrt{\left(g + V\dot{\theta}_{\text{cmd}}\right)^2 + \left(V\cos\theta\dot{\psi}_{\text{cmd}}\right)^2}}\right) + \arctan\left(-\frac{g + V\dot{\theta}_{\text{cmd}}}{V\cos\theta\dot{\psi}_{\text{cmd}}}\right) \tag{136}$$

where the commanded track rate is adjusted for level turns: $\dot{\psi}_{\text{cmd}} = \dot{\chi}_{\text{cmd}}\cos\theta$.

This result is achieved by using the universal relationship:

$$a\sin\phi - b\cos\phi = c \quad \Longleftrightarrow \quad \phi = \arccos\left(\frac{c}{\sqrt{a^2 + b^2}}\right) + \arctan\left(-\frac{a}{b}\right) \tag{137}$$

Eq. (136) was validated for specific situations of straight sideslipping flight, where it simplifies to $\phi_{\text{cmd}} = \arcsin\left(-n_Y\right)$ and for level turn coordinated (zero sideslip) flight, where it simplifies to $\phi_{\text{cmd}} = \arctan\left(\dot{\psi}_{\text{cmd}}\frac{V}{g}\right)$. The commanded bank angle value ϕ_{cmd} from Eq. (136) is then fed to the bank control outer loop control system (VI.E.2).

Track Rate By Lateral Translation:

For track rate by lateral translation, the commanded track rate is used to compute the commanded lateral velocity:

$$V_{Y_{\text{cmd}}} = \tau_\chi \dot{\chi}_{\text{cmd}} \tag{138}$$

where 1 deg of track angle corresponds to 1 ft/sec of lateral velocity. The lateral velocity command is sent to the lateral component of the translational rate command outer loop control system (VI.E.12).

12. Translational Rate Control (TRC)

Translational Rate Command is a dedicated mode which is used in the hover mode and for precision maneuvering with respect to the ground. Longitudinal and lateral stick deflections command the forward and sideways inertial speed components respectively. The derivation of how the lateral inertial speed component maps to roll angle is shown below. Pitch angle is not used here for controlling the forward inertial speed component, since a more efficient pusher propeller is available, which eliminates the need to pitch for speed.

This kinematic relationship shows how the translational rate components are related to the Euler angles[22]:

$$\begin{bmatrix} \ddot{x}_{\text{gnd}} \\ \ddot{y}_{\text{gnd}} \\ \ddot{z}_{\text{gnd}} \end{bmatrix} = \begin{bmatrix} 0 \\ 0 \\ g \end{bmatrix} + \frac{1}{m} \mathbf{\Omega}_{\psi}^{-1} \mathbf{\Omega}_{\theta}^{-1} \mathbf{\Omega}_{\phi}^{-1} \left(\begin{bmatrix} \bar{q} S C_{X_B} \\ \bar{q} S C_{Y_B} \\ \bar{q} S C_{Z_B} \end{bmatrix} + \begin{bmatrix} T \cos \delta_T \\ 0 \\ T \sin \delta_T \end{bmatrix} \right) \tag{139}$$

where the body force components are defined by the aerodynamic forces as follows:

$$\begin{bmatrix} \bar{q} S C_{X_B} \\ \bar{q} S C_{Y_B} \\ \bar{q} S C_{Z_B} \end{bmatrix} = \bar{q} S \mathbf{\Omega}_{\alpha}^{-1} \mathbf{\Omega}_{\beta}^{-1} \begin{bmatrix} -C_{D_{\text{aero}}} \\ C_{Y_{\text{aero}}} \\ -C_{L_{\text{aero}}} \end{bmatrix} \tag{140}$$

Simplifying by assuming that only the vertical rotors are used in the hover phase and that the aerodynamic influences are negligible due to the low airspeed, results in:

$$m \mathbf{\Omega}_{\psi} \begin{bmatrix} \ddot{x}_{\text{gnd}} \\ \ddot{y}_{\text{gnd}} \\ \ddot{z}_{\text{gnd}} - g \end{bmatrix} = \mathbf{\Omega}_{\theta}^{-1} \mathbf{\Omega}_{\phi}^{-1} \begin{bmatrix} 0 \\ 0 \\ T \sin \delta_T \end{bmatrix} \tag{141}$$

Expanding these matrix equations results in:

$$\begin{bmatrix} m \left(\ddot{x}_{\text{gnd}} \cos \psi + \ddot{y}_{\text{gnd}} \sin \psi \right) \\ m \left(\ddot{y}_{\text{gnd}} \cos \psi - \ddot{x}_{\text{gnd}} \sin \psi \right) \\ m \left(\ddot{z}_{\text{gnd}} - g \right) \end{bmatrix} = \begin{bmatrix} \cos \phi \sin \theta T \sin \delta_T \\ - \sin \phi T \sin \delta_T \\ \cos \phi \cos \theta T \sin \delta_T \end{bmatrix} \tag{142}$$

Solving for bank angle ϕ results in:

$$\sin \phi = - \frac{m \left(\ddot{y}_{\text{gnd}} \cos \psi - \ddot{x}_{\text{gnd}} \sin \psi \right)}{T \sin \delta_T} \tag{143}$$

Besides it can be found that:

$$m \left\| \begin{matrix} \ddot{x}_{\text{gnd}} \\ \ddot{y}_{\text{gnd}} \\ \ddot{z}_{\text{gnd}} - g \end{matrix} \right\|_2 = \left\| \begin{matrix} 0 \\ 0 \\ T \sin \delta_T \end{matrix} \right\|_2 \tag{144}$$

And thus:

$$T \sin \delta_T = m \sqrt{\ddot{x}_{\text{gnd}}^2 + \ddot{y}_{\text{gnd}}^2 + \left(\ddot{z}_{\text{gnd}} - g \right)^2} \tag{145}$$

Implementing Eq. (145) in Eq. (143) results in the following equation for required bank angle based on the required translational accelerations, which is independent of any airframe information:

$$\phi_{\text{req}} = - \arcsin \frac{\left(\ddot{y}_{\text{gnd}_{\text{req}}} \cos \psi - \ddot{x}_{\text{gnd}_{\text{req}}} \sin \psi \right)}{\sqrt{\ddot{x}_{\text{gnd}_{\text{req}}}^2 + \ddot{y}_{\text{gnd}_{\text{req}}}^2 + \left(\ddot{z}_{\text{gnd}_{\text{req}}} - g \right)^2}} \tag{146}$$

As was illustrated in Fig. 10, this required bank angle is first fed to the bank control system as discussed in Sec. VI.E.2, whose output is then fed to the roll rate control system in Sec. VI.E.8, and that output finally feeds to the rate command attitude hold control system which is discussed in Sec. VI.F.3.

The required forward vehicle referenced acceleration component along the body X-axis is calculated as follows:

$$\dot{u}_{\text{gnd}_{\text{req}}} = \ddot{x}_{\text{gnd}_{\text{req}}} \cos \psi + \ddot{y}_{\text{gnd}_{\text{req}}} \sin \psi \tag{147}$$

and fed to the acceleration inner loop control system which is discussed in Sec. VI.F.1.

Because of the relative degree, the linear controllers of the two TRC channels work up to the second order derivative, and they have the following control law:

$$\nu_{\ddot{x}} = \ddot{x}_{\text{gnd}_{\text{req}}} = \left(K_{\dot{x}} + \frac{K_{\dot{x}_I}}{s}\right)\left(\dot{x}_{\text{gnd}_{\text{ref}}} - \dot{x}_{\text{gnd}}\right) + K_{\ddot{x}}\left(\ddot{x}_{\text{gnd}_{\text{ref}}}\right) \tag{148}$$

$$\nu_{\ddot{y}} = \ddot{y}_{\text{gnd}_{\text{req}}} = \left(K_{\dot{y}} + \frac{K_{\dot{y}_I}}{s}\right)\left(\dot{y}_{\text{gnd}_{\text{ref}}} - \dot{y}_{\text{gnd}}\right) + K_{\ddot{y}}\left(\ddot{y}_{\text{gnd}_{\text{ref}}}\right) \tag{149}$$

$$\nu_{\ddot{z}} = \ddot{z}_{\text{gnd}_{\text{req}}} = K_{\dot{z}}\left(\dot{z}_{\text{gnd}_{\text{req}}} - \dot{z}_{\text{gnd}}\right) \tag{150}$$

The values of the controller gains mentioned in Eq. (148)–(150) are specified in Table 1. The second order time derivatives of the control commands used in Eq. (148)–(150) are fed forward internal signals from the first order reference models for the two TRC channels:

$$H_{\text{ref}}(s) = \frac{1}{\tau_{\text{TRC}}s + 1} \tag{151}$$

The value for the time constant in Eq. (151) is $\tau_{\text{TRC}} = 2.57s$ and was chosen such that the reference model satisfies the ADS-33 Flying and Handling Quality requirements. Fig. 34 shows the interconnections between reference model, linear controller and kinematics inversion for TRC.

Table 1 Linear controller gains for Eq. (148)–(150)

axis	rate	acceleration
longitudinal & lateral	$K_{\dot{x}/\dot{y}/\dot{z}} = 2 * 0.25$ $K_{\dot{x}/\dot{y}_I} = 0.25^2$	$K_{\ddot{x}/\ddot{y}} = 1$
yaw	$K_{\psi} = 6$	$K_{\dot{\psi}} = 5$

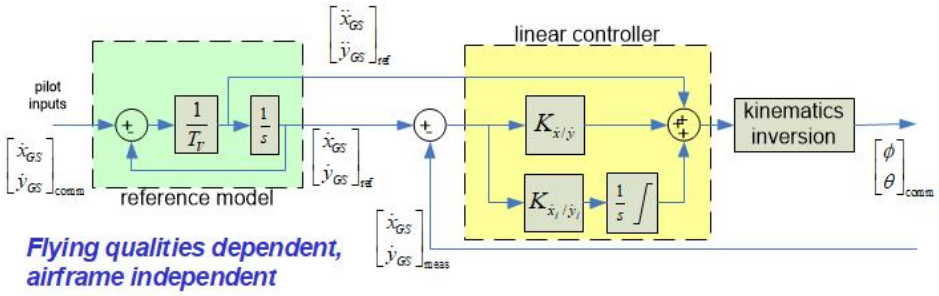

Fig. 34 Detailed overview of the control structure and interconnections for TRC (translational rate control)

13. Vertical Speed Control

For vertical speed control, the commanded vertical speed $\dot{h}_{\text{cmd}}$ is used to control the vertical speed either by heave (in the hover regime) or by pitch (in the forward flight and transitional regimes).

Vertical Speed By Heave:

For vertical speed by heave, the commanded vertical speed is passed directly to the RCHH inner loop control system (VI.F.5).

Vertical Speed By Pitch:

For vertical speed by pitch, the commanded vertical speed is used to calculate the commanded flight path angle γ_{cmd}:

$$\gamma_{\text{cmd}} = \arctan\frac{\dot{h}_{\text{cmd}}}{V_{\text{gnd}_{\text{lim}}}} \tag{152}$$

where $V_{\text{gnd}_{\text{lim}}}$ is the singularity protected ground speed:

$$V_{\text{gnd}_{\text{lim}}} = \max\left(V_{\text{gnd}}, 10kts\right) \tag{153}$$

Next the commanded flight path rate $\dot{\gamma}_{\text{cmd}}$ is calculated, based on the flight path angle time constant τ_γ, using Eq. 122. The commanded pitch rate is approximated to be equal to the commanded flight path angle rate (i.e., $\dot{\theta}_{\text{cmd}} \approx \dot{\gamma}_{\text{cmd}}$), and the resulting the pitch rate command is sent to the pitch rate control outer loop control system (VI.E.7).

F. Inner Loop Control Modes

There inner loop control modes introduced in Fig. 11 are explained below. The inner loop control system corresponding to each mode generally consists of a reference model and an error controller (Fig. 35). This setup allows for decoupling of the gain tuning according to the purpose. The gains in the reference model serve for command shaping, i.e. the responsiveness of the vehicle to a commanded input. The PID gains of the error controller tune how quick disturbances (such as gust and turbulence induced deviations) are compensated for.

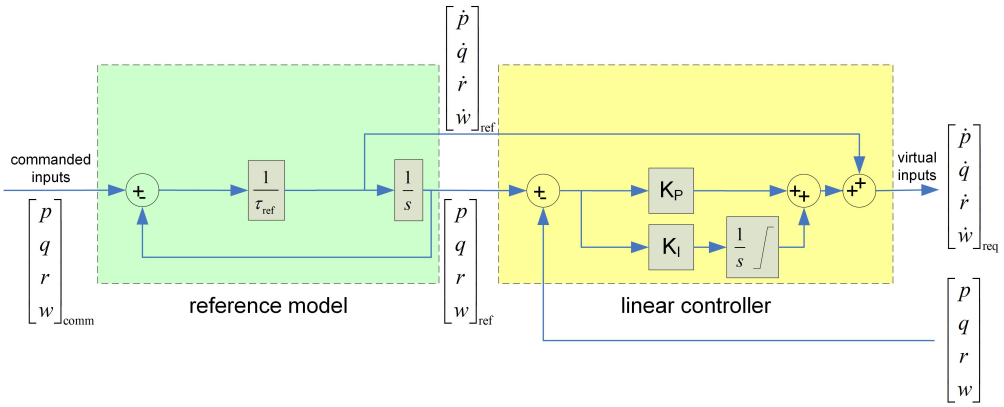

Fig. 35 Block diagram of command filtering, reference model and linear controller

1. Acceleration Command Speed Hold (ACSH)

This acceleration command system is basically a pure integral action based linear controller that makes use of the error between the commanded speed rate of change $\dot{V}_{\text{cmd}}$ and the computed speed rate of change $\dot{V}_{\text{comp}}$ for calculating the required linear acceleration for the dynamic inversion loop:

$$\dot{u}_{\text{req}} = \dot{V}_{\text{ref}} = \frac{1}{\tau_u}\left(\dot{V}_{\text{cmd}} - \dot{V}_{\text{comp}}\right) dt \tag{154}$$

This computed speed rate of change switches from the calibrated airspeed rate of change (in the forward flight and transitional regimes), to the forward ground speed rate of change $\dot{u}_{\text{gnd}}$ (in the hover regime).

2. Angle of Attack Command (AOAC)

The Angle Of Attack Command module (AOAC) basically calculates a commanded body fixed vertical speed w_{cmd}, based on the maximum allowed angle of attack α_{max} and the body fixed forward speed u_b:

$$w_{\text{cmd}} = \tan\alpha_{\text{max}} \cdot u_b \tag{155}$$

This maximum angle of attack α_{max} value can change depending on the flight regime. Next, this commanded vertical speed w_{cmd} is fed through its respective rate command module as discussed in Fig. 35, resulting in a required vertical acceleration $\dot{w}_{\text{req}}$, to be fed to the respective dynamic inversion calculation.

3. Rate Command Attitude Hold (RCAH)

Rate Command Attitude Hold is a variation of ACAH, where the commanded inputs are body fixed roll and pitch rates p_{cmd} and q_{cmd}. This mode is used in the cruise forward flight phase. This command shaping consists of a first order reference model with the corresponding time constant τ_{ref}. This reference model is connected to a linear PI controller. The angular and linear accelerations from the first order reference model $\dot{p}_{\text{ref}}$ and $\dot{q}_{\text{ref}}$ are fed forward and added to the linear controller output to minimize lag between response and reference signal. Required body angular accelerations $\dot{p}_{\text{req}}$ and $\dot{q}_{\text{req}}$ are the output of the linear controller, to be fed to the dynamic inversion calculation. Fig. 35 illustrates the interconnections between commanded inputs, reference model and controller for this control mode.

Subsequent modes, such as Rate Command Direction Hold (RCDH), Rate Command Height Hold (RCHH), Angle Of Attack Command (AOAC) and Turn Coordination (TC) have a similar setup as RCAH, but then with the controlled variables body fixed yaw rate r_{cmd} and vertical speed w_{cmd}, as also shown in Fig. 35, supplemented by a few additional coordinate transformations as elaborated in the paragraphs below.

4. Rate Command Direction Hold (RCDH)

Rate Command Direction Hold is similar to RCAH. A steady commanded earth referenced yaw rate commands a steady rate of change of the heading. This mode is used in the hover and landing phases of flight.

In this case the commanded input is the earth referenced rate of change of the heading $\dot{\psi}_{\text{cmd}}$, which is transformed in a commanded body fixed yaw rate r_{cmd}, based on the following inverse Euler equation:

$$r_{\text{cmd}} = \dot{\psi}_{\text{cmd}} \cos\theta \cos\phi - \dot{\theta} \sin\phi \tag{156}$$

Next, this commanded yaw rate r_{cmd} is fed through its respective rate command module as discussed in Fig. 35, resulting in a required yaw angular acceleration $\dot{r}_{\text{req}}$, to be fed to the dynamic inversion calculation.

5. Rate Command Height Hold (RCHH)

Rate Command Height Hold is similar to the both previous ones. A steady height rate command results in a steady climb or sink rate. This mode is used in lower speed flight regimes.

In this case, the commanded input is the earth referenced height rate of change $\dot{h}_{\text{cmd}}$, which is transformed in a commanded body fixed vertical speed component w_{cmd} as follows:

$$w_{\text{cmd}} = \frac{1}{\cos\phi \cos\theta} \left(-\dot{h}_{\text{cmd}} + \sin\theta \cdot u_b + \sin\phi \cos\theta \cdot v_b \right) \tag{157}$$

Next, this commanded vertical speed w_{cmd} is fed through its respective rate command module as discussed in Fig. 35, resulting in a required vertical acceleration $\dot{w}_{\text{req}}$, to be fed to the dynamic inversion calculation.

For the feedback path in the linear controller, one needs to compute the vertical speed in body axes from vertical speed in earth fixed axes (to incorporate vertical winds, etc.)

$$w_b = \frac{1}{\cos\phi \cos\theta} \left(\dot{z} + \sin\theta \cdot u_b + \sin\phi \cos\theta \cdot v_b \right) \tag{158}$$

6. Turn Coordination (TC)

For turn coordination, sideslip β control has been implemented as outer loop over rate control according to the following control law:

$$r_{\text{cmd}} = -K_\beta \left(\beta_{\text{cmd}} - \beta \right) + r_{\text{TC}} \tag{159}$$

where the controller gain $K_\beta = \frac{\omega_r}{3}$. In Eq. (159), yaw rate for turn coordination r_{TC} is calculated as follows:

$$r_{\text{TC}} = \sin\phi \cos\theta \cdot \frac{g_0}{V_{\text{TAS}_{\text{lim}}}} \tag{160}$$

where the denominator $V_{\text{TAS}_{\text{lim}}}$ is singularity protected as follows:

$$V_{\text{TAS}_{\text{lim}}} = \max\left(V_{\text{TAS}}, 10 \text{ kts} \right) \tag{161}$$

Next, this commanded yaw rate r_{cmd} is fed through its respective rate command module as discussed in Fig. 35, resulting in a required yaw angular acceleration $\dot{r}_{\text{req}}$, to be fed to the dynamic inversion calculation.

References

[1] VFS, "eVTOL Aircraft Directory," Online, 2022. URL https://evtol.news/aircraft/, retrieved March 20, 2022.

[2] Malpica, C., and Withrow-Maser, S., "Handling Qualities Investigation of Variable Blade Pitch and Variable Rotor Speed Controller eVTOL Quadrotor Concepts for Urban Air Mobility," *Proceedings of the VFS International Powered Lift Conference*, Vertical Flight Society, 2020.

[3] "A Rational Construct for Simplified Vehicle Operations (SVO)," Gama epic svo subcommittee whitepaper, Washington D.C. and Brussels, Belgium, May 2019. URL https://gama.aero/documents/svo-whitepaper-a-rationale-construct-for-simplified-vehicle-operations-svo-version-1-0-may2019/.

[4] Nicholas, O. P., and Bennett, P. J., "Proposed Wide Envelope Unified Control Concept for Vectored Thrust VSTOL Aircraft," Technical Memorandum FS312, Royal Aircraft Establishment RAE, Mar. 1980.

[5] Scott, R., *Aeroplane Monthly*, Key Publishing, 2020, Vol. 48, Chaps. VAAC HARRIER: How the oldest two-seat Harrier helped perfect the control method for today's F-35 Lightning II, pp. 92 – 99.

[6] Denham, J., "STOVL Integrated Flight and Propulsion Control: Current Successes and Remaining Challenges," *2002 Biennial International Powered Lift Conference and Exhibit*, American Institute of Aeronautics and Astronautics, 2002. doi:10.2514/6.2002-6021.

[7] Denham, J., and Paines, J., "Converging on a Precision Hover Control Strategy for the F-35B STOVL Aircraft," *AIAA Guidance, Navigation and Control Conference and Exhibit*, American Institute of Aeronautics and Astronautics, 2008. doi:10.2514/6.2008-6331.

[8] Stewart, E., "A piloted simulation study of advanced controls and displays for novice general aviation pilots," *32nd Aerospace Sciences Meeting and Exhibit*, American Institute of Aeronautics and Astronautics, 1994. doi:10.2514/6.1994-276.

[9] Kaneshige, J., Lombaerts, T., Shish, K., and Feary, M., "Command and Control Concepts for a Lift Plus Cruise Electric Vertical Takeoff and Landing Vehicle," *AIAA AVIATION 2023 FORUM*, American Institute of Aeronautics and Astronautics, 2023. doi:10.2514/6.2023-3910.

[10] Feary, M., Kaneshige, J., Haworth, L., Lombaerts, T., Shish, K., Iwai, N., and Archdeacon, J., "Evaluation of Novel V/STOL Aircraft Control for Expected AAM Operations," *AIAA AVIATION 2023 FORUM*, American Institute of Aeronautics and Astronautics, 2023. doi:10.2514/6.2023-3909.

[11] Lombaerts, T., Kaneshige, J., and Feary, M., "Control Concepts for Simplified Vehicle Operations of a Quadrotor eVTOL Vehicle," *AIAA AVIATION 2020 FORUM*, American Institute of Aeronautics and Astronautics, 2020. doi:10.2514/6.2020-3189.

[12] Silva, C., Johnson, W. R., Solis, E., Patterson, M. D., and Antcliff, K. R., "VTOL Urban Air Mobility Concept Vehicles for Technology Development," *2018 Aviation Technology, Integration, and Operations Conference*, American Institute of Aeronautics and Astronautics, 2018. doi:10.2514/6.2018-3847.

[13] Val, R. D., and He, C., "FLIGHTLAB^{TM} Modeling for Real Time Simulation Applications," *International Journal of Modeling Simulation and Scientific Computing*, Vol. 08, No. 4, 2017. doi:10.1142/S1793962317430036.

[14] Val, R. D., and He, C., "Validation of the FLIGHTLAB virtual engineering toolset," *The Aeronautical Journal*, Vol. 122, No. 1250, 2018, pp. 519–555. doi:10.1017/aer.2018.12.

[15] Zivan, L., and Tischler, M. B., "Development of a full flight envelope helicopter simulation using system identification," *Journal of the American Helicopter Society*, Vol. 55, No. 2, 2010. doi:10.4050/JAHS.55.022003.

[16] Tobias, E. L., Sanders, F. C., and Tischler, M. B., "Full-envelope stitched simulation model of a quadcopter using STITCH," *AHS International 74th Annual Forum & Technology Display*, Vertical Flight Society, 2018.

[17] "Realistic Gusting Crosswind Profiles for Flight Simulation Training Device (FSTD) Qualification," Tech. Rep. NSP GB 16-02, Federal Aviation Administration (FAA), May 2019. URL https://www.faa.gov/sites/faa.gov/files/about/initiatives/nsp/fstd_dir/16-02.pdf.

[18] "Aeronautical Design Standard, Performance Specification, Handling Qualities Requirements for Military Rotorcraft," Tech. Rep. ADS-33E-PRF, United States Army Aviation and Missile Command Aviation Engineering Directorate, Mar. 2000. URL https://www.amrdec.army.mil/amrdec/rdmr-se/tdmd/Documents/ads33front.pdf.

[19] Lombaerts, T., Kaneshige, J., Schuet, S., Hardy, G., Aponso, B. L., and Shish, K. H., "Nonlinear Dynamic Inversion Based Attitude Control for a hovering quad tiltrotor eVTOL vehicle," *AIAA Scitech 2019 Forum*, American Institute of Aeronautics and Astronautics, 2020. doi:10.2514/6.2019-0134.

[20] Lombaerts, T., Kaneshige, J., Schuet, S., Aponso, B. L., Shish, K. H., and Hardy, G., "Dynamic Inversion based Full Envelope Flight Control for an eVTOL Vehicle using a Unified Framework," *AIAA Scitech 2020 Forum*, American Institute of Aeronautics and Astronautics, 2020. doi:10.2514/6.2020-1619.

[21] Archdeacon, J. L., and Iwai, N., "Aerospace Cognitive Engineering Laboratory (ACELAB) Simulator for Urban Air Mobility (UAM) Research and Development," *AIAA AVIATION 2020 FORUM*, American Institute of Aeronautics and Astronautics, 2020. doi:10.2514/6.2020-3187.

[22] Simplicio, P., Pavel, M., van Kampen, E., and Chu, Q., "An acceleration measurements-based approach for helicopter nonlinear flight control using Incremental Nonlinear Dynamic Inversion," *Control Engineering Practice*, Vol. 21, 2013, pp. 1065–1077. doi:10.1016/j.conengprac.2013.03.0009.